CERN/SPSLC 96–50
SPSLC/R110
October 18, 1996

Technical Note on the NA45/CERES Upgrade

P. Holl, H. Kraner, P. Rehak
Brookhaven National Laboratory, Upton, USA

J. Schukraft
CERN, Geneva, Switzerland

P. Braun-Munzinger, D. Miskowiec, V. Pantuev
GSI, Darmstadt, Germany

G. Agakichiev, Y. Minaev, Y. Panebrattsev, S. Razin, S. Shimanskij, V. Yurevich
JINR, Dubna, Russia

F. Ceretto, Ch. Fuchs, O. Nix, J. Rak, J.P. Wurm
Max-Planck-Institut für Kernphysik, Heidelberg, Germany

E. Gatti, M. Sampietro
Politecnico di Milano, Italy

H. Appelshäuser, R. Baur, A. Drees, P. Ernst, S. Esumi, P. Glässel, A. Huber, Ch. Jung, B. Lenkeit, M. Messer, A. Pfeiffer, M. Richter, B. Schmitz, W. Seipp, H.J. Specht, J. Stachel, C. Voigt, C. Weber, J.P. Wessels, T. Wienold
Universität Heidelberg, Germany

Z. Fraenkel, I. Ravinovich, E. Sokol, G. Tel-Zur,
I. Tserruya (Spokesman)
Weizmann Institute, Rehovot, Israel

1 Introduction

In a recent Addendum to the NA45/CERES Proposal we described an upgrade of the experiment by the addition of a radial TPC with an additional magnetic field after the existing RICH spectrometer. This will significantly improve the di-electron mass resolution which is dominated by momentum resolution. The goal is to achieve a momentum resolution which allows the experiment to be sensitive to the width of e.g. the ω meson at the level of its natural width of 8.4 MeV/c^2.

The TPC is located immediately downstream of RICH2 and covers in beam direction z = 3.55 - 5.05 m (see Figure 1). The magnetic field is provided by two large coils surrounding the TPC with currents running in opposite direction (CERES Note 150). This will deflect charged particles in azimuthal direction. Measurement of the track curving through the magnetic field in the TPC will provide the momentum information. The opening angle between the two electrons of the pair is measured just behind the target in two Silicon drift chambers with sufficient resolution to not affect the mass resolution of relevance for CERES (see CERN/SPSLC 96-35/P280 Add.1). The geometric acceptance of the radial TPC will follow the acceptance of the upstream RICH spectrometer and covers polar angles θ from 8.0 to 14.5 degrees. The drift will take place in a radial electric field with field strength proportional to 1/r. For simplicity we envision a cylindrical geometry for the TPC with an inner radius (of the active volume) of 0.50 m and an outer radius of 1.31 m.

In this note we describe the present status of the technical aspects of the proposed upgrade. In section 2 the geometrical and field configuration are briefly summarized. Section 3 describes the magnetic coil system. The lay-out and performance of the TPC are described in section 4, along with a discussion of the overall mass resolution and its impact on the physics goals. The TPC read-out electronics is discussed in section 5. Finally, in section 6 we give the schedule envisioned for the upgrade.

2 Geometrical and field configuration

Figure 1 shows a schematic view of the radial TPC and the read-out chamber. The negative charge drifts to the outside of the cylinder where it is detected in a barrel of cathode pad chambers. At present it is forseen to segment the read-out chamber into 16 individual (identical) elements of approximate size of 52 $\times$ 150 cm. The read-out cell geometry is given by alternating sense and field wires spaced 5 mm apart and located 5 mm above a cathode pad plane with pad size of 10 mm. At present we envision pads of the 'displaced single chevron' type (B. Yu, Ph.D. Thesis, U. of Pittsburgh, 1991; B. Yu, G.C. Smith, V. Radeka and E. Mathieson, IEEE Trans. Nucl. Sci. 38 (1991) 454), a design that was successfully used for a pair of vertex chambers in E877 at the Brookhaven AGS (R.A. Bersch, Master Thesis, SUNY Stony Brook, May 1995). Since occupancy is not a problem 4 adjacent pads (in z) will be ganged together before the preamplifier to save electronics channels. In z-direction there are 14 such groups of 4 pads each, i.e. there will be 14 measurements of each track along z.

The magnetic field lines in the r-z plane relevant in the region of the TPC are indicated in Figure 2. The two new coils are located at z = 3.8 and 4.5 m. The dash-dotted line marks the acceptance in polar angle θ of the upstream spectrometer as well as of the TPC (location indicated by the short-dashed rectangle). More details about the magnet coils can be found in section 3.

Figure 3 shows the radial and longitudinal components of the magnetic field both at the inner and outer end of the acceptance in θ as a function of the z-coordinate. Also shown is the trajectory of a singly positively charged particle with momentum 1 GeV/c on the surface of a cone with angle θ again for the minimum and maximum θ accepted (Figure 3, bottom). The plot shows the distance, on the surface of a cone, from the location of a track without magnetic field. In addition we show in Figure 3 the quantity that determines the extent of the primary ionization trail in direction of the wires of the read-out chambers, $r \cdot d\phi/dz$. This quantity needs to be multiplied with the length Δz covered by each read-out pad (presently 4 cm). The kinks at $z \approx 1.2$ m are due to the two super-conducting magnet coils located between the two RICH counters, the strong bend at $z \approx 4.2$ m, *i.e.* approximately in the middle of the TPC, represents the region of maximal radial field strength produced by the new coils.

The electrostatic potential and electric field strength as functions of r are shown in Figure 4. The field configuration shown implies a field cage with a potential of 15 kV at the inner surface of the cylinder and ground potential at the outer surface where the read-out chambers are located. We will, however, lay out the field cage and HV system for a maximum voltage of 30 kV and will study the running conditions at a higher electric field. To illustrate the advantage of this we note that at a potential of 20 kV the maximum drift time drops to 60 μs *vs.* 71 μs at 15 kV for our present choice of drift gas.

3 The magnetic coil system of the CERES TPC

This section contains some specifications and considerations for the new magnet coils.

The magnet system for the proposed TPC consists of two closely spaced short solenoids with opposite sense currents. The resulting field is shown in Figure 2. The axial geometry of the TPC and its magnet are optimally adapted to the CERES acceptance (8 to 14.5 deg lab angle with full 2π coverage of azimuth) since deflected particles, to first order, stay within the acceptance.

In view of the limited running period, the design foresees conventional water-cooled copper coils. Table 1 lists some specifications of the coils.

In accordance to the power supply foreseen, a 28×28 mm^2 Cu conductor with a 15 mm water bore is foreseen, operated at 3200 A. This gives a current density similar to the one of the existing warm coils of the CERES spectrometer. The coils are to be operated in series.

The Dubna group of CERES is interested in the production of the coils and has already given a first tentative quotation based on these preliminary specifications, along with a firm committment to deliver the system within the foreseen time and cost estimate. The dimensions of the coils are such that ordinary road transport is feasible with the coils mounted upright.

Coil Specifications (preliminary)

		coil 1	coil 2
inner radius	mm	1420	1420
outer radius	mm	1800	1920
length	mm	290	480
windings		10×13	16×17
z-position of center	mm	3750	4550
current	kA$\times$turns	416	870
Cu mass	t	7.2	15.7

Power supply

In recent discussions with G. Fernquist and J.C. Carlier at CERN it turned out that there is an old SPS power supply with a rating of 3300 A/500 V which would just fit and which could be reactivated at a cost of about 40 kCHF – mainly for control electronics (the cost for a new power supply would be about 350 kCHF). The total power dissipation of the new magnet with the preliminary specifications above at 3200 A is 1.42 MW, voltage drop is 443 V, well matched to this power supply.

The RICH spectrometer will keep its present power supply, allowing independent current settings for the RICH and the TPC systems. In this context, it is interesting to note that the compensation of the field of the two TPC coils in the region of the RICH2 radiator – ensuring straight tracks there – is *independent* of the current setting in the RICH spectrometer.

Mechanical support structure

The support structure for the coils is not a simple task. It must satisfy the following needs:

- support the weight of the coils (about 23 t according to the present specifications),
- ensure a fixed position with respect to the RICH system,
- take the forces between the two coils (of the order of 100 t axial *repulsion*),
- take the attractive force towards the RICH magnet system,
- provide accurate positioning of the TPC in an appropriate mount. For servicing, the TPC has to be movable.

Figure 5 shows a side view of the downstream end of the RICH spectrometer with the location of the new coil pair. The platform presently carrying the CERES spectrometer will have to be modified. A view against the beam is shown in Figure 6, it demonstrates that the main longitudinal support beams of the platform do not directly interfere with the coils. The question of distortions of the field by these steel profiles has to be assessed, however, in case they are not removed for other reasons.

It is clear that the platform cannot reasonably take the weight of the new coils without additional legs to the floor (the downstream floor support of the platform is visible in Figure 5, the other one is located $\sim$3 m upstream of it). An alternative is a support that itself sits on the floor. The – normally attractive – forces between the RICH magnet system and the TPC coils require a connection between the support and the RICH-2 vessel. This connection must also work in case of wrong relative current senses in RICH and TPC coils, if this cannot safely be prevented by interlocks.

To insure integration into the present CERES setup it is our preferred option to build the support for the magnet coils at CERN. In a first discussion with Mr Heuzey (CERN), the costs were estimated at 30 to 40 kCHF, including the modification of the existing platform of CERES.

4 TPC layout and performance

4.1 General design considerations

In the following, we briefly summarize the criteria for TPC design and choice of gas.

- Although the azimuthal (ϕ) deflection of a track at smaller polar angle θ is smaller because of the smaller magnetic field, the projected deflection of the track onto the read-out chamber on the outside cylinder will be the same for different θ, since the momentum kick projected onto the r-ϕ plane is constant for different θ and the electrons drift radially outward following the radial electric field. This is the merit of the radial TPC.
- On the other hand, the diffusion of the electron cloud is larger when it originates from the inner region of the drift volume, corresponding to smaller θ. In addition to this, the diffusion is enlarged by the effect of the radial geometry.
- Increasing the total number of primary electrons allows to improve the position resolution given by the centroid calculation on the read-out pad chamber.
- Another criterion for good momentum resolution is that the radiation length of the gas has to be such that multiple scattering does not impair the resolution.
- The two magnet coils will also produce a longitudinal component of the magnetic field which will lead to a spiralling motion of the electrons in the r-ϕ plane superimposed to the radial drift. This Lorentz angle will deteriorate the position resolution for a given time slice measured by a flash-ADC.
- Finally, the drift velocity has to be chosen such that it does not limit the interaction rate and therefore the beam intensity which is required to achieve the goal of 25-30 k electron pairs with invariant mass above 200 MeV/c^2 for a six week running period. The beam rate envisioned is 1.5 - 2 $\cdot 10^6$/burst.

To achieve the desired momentum resolution in the design of the radial TPC, the gas was optimized for small diffusion, small Lorentz angle, large ionization, long radiation length, and reasonably fast drift velocity keeping in mind that the electric field should not significantly exceed 0.3 kV/cm.

4.2 Calculation of drift gas properties

Calculations of the properties of various gas mixtures were performed using the codes Garfield (version 5.32) and Magboltz (version 1.10). For a large number of gas mixtures the drift velocity, Lorentz angle, longitudinal, and transverse diffusion coefficients were calculated for a given electric and magnetic field at fixed angle between them. The calculations cover magnetic field strength from 0 to 0.5 T at angles between 0 and 90 degrees with respect to the electric field. Figure 7 shows results for various noble gas/CO_2 mixtures for the most difficult case of a magnetic field of 0.5 T perpendicular to E (as can be seen in Figure 3, there is only a small region in z and θ where we will have to deal with such conditions). The gas mixtures under consideration are Ne/CO_2, He/CO_2 and Ar/He/CO_2 with CO_2 admixtures of 10 and 20 % and a noble gas content of 90 or 80 % respectively. Also shown in the bottom of Figure 7 are the diffusion coefficients normalized to the square root of the number n_e of primary electrons since this ratio is the relevant quantity for the position resolution at the read-out pad chamber.

The conventional mix of Ar and CH_4 in the ratio of 90 : 10 is not acceptable for our purpose. The multiple scattering in Ar-dominated mixtures deteriorates the momentum resolution too much (for us the most relevant momentum range is 2 - 3 GeV/c). Furthermore, the Lorentz angle is very large (60-70 deg. in the relevant field range) and diffusion is large. The latter two problems can be cured by adding small amounts of CO_2 to the mixture as shown experimentally by Alber et al. (Nucl. Instr. Methods A349, 56(1994)). In terms of multiple scattering, mixtures with 50 % or less Ar or any fraction of Ne or He are acceptable. This is the baseline of the selection shown in Figure 7. Mixtures dominated by He have rather low ionization and a drift velocity that is low. As will be shown later the ionization in 4 cm gas is still sufficient to not dominate the momentum resolution in our case. However, drift times in excess of 100 μs combined with the required beam intensity make them not the preferred solution for our application, leaving for consideration mixtures of Ne or He/Ar with CO_2. Increasing the CO_2 content decreases the Lorentz angle und reduces the diffusion, *i.e.* improves the position resolution. However, at the same time, the drift velocity drops. It appears that a good compromise is a mixture with a 10 % CO_2 content.

A maximum drift time of 71 μs makes Ne/CO_2 the preferred solution. He/Ar/CO_2 has the advantage of lower cost and yields, in terms of resolution, very similar performance but with a maximum drift time of 98 μs. In Figure 8 is displayed the rate of clean interactions as a function of beam intensity. There 'clean' is defined to mean no further interaction within $\pm$ the drifttime. At the desired beam rate of $5 \cdot 10^5$/s ($2 \cdot 10^6$/burst) the loss in going from Ne/CO_2 to He/Ar/CO_2 (both with 90 % noble gas) is only 15 % in the number of events. Going to a mixture with He/Ar/CO_2 in the ratio 40:40:20, the rate of clean events at the same beam intensity is reduced more severely to 2/3. Should it turn out that other factors in the experiment limit the beam rate to lower values we will consider to increase the CO_2 content to a maximum of 20 % to further improve resolution. These considerations indicate that the TPC rate capability is not a limiting factor for the luminosity of the experiment.

4.3 Electron drift

By using an electric and magnetic field map in the TPC drift volume and the gas properties as shown in Figure 7, the drift path of the electrons and the diffusion of the cloud are calculated. Figure 9 shows the electron drift in the r-ϕ plane at four different z-positions.

The distance between adjacent points in Figure 9 corresponds to 10 μs drift time. The dashed circles indicate the 8 - 14.5 degree acceptance in θ while the solid circles mark the TPC boundaries. For each z-position 8 different trajectories (displaced in ϕ by 45 degrees in Figure 9) are drawn corresponding to drift starting at 8, 9, 10, ... degrees in θ. The drift gas used for this calculation is our baseline choice of Ne(90 %)/CO_2(10 %).

Figure 10 shows the diffusion of the electron cloud in transverse and longitudinal direction for 4 different z-positions as a function of the drift time. As in Figure 9 results are shown for drift starting at θ = 8, 9, 10, ... degrees and different calculations are displaced by 10 μs relative to each other for better visibility. The gas used for the calculation is the same as above. For the transverse diffusion, the effect of the radial geometry is taken into account.

By repeating this calculation for locations all over the active volume in the acceptance, a map was produced of the width σ of the charge cloud at the sense wire position. The calculations take into account the width of the charge cloud due to diffusion (σ_t) as well as to dϕ/dz (σ_α) as shown in Figure 3. This latter term is caused by the so called $\tan\alpha$ effect. The effect of the finite Lorentz angle is considered at a later stage as a contribution to the ϕ resolution.

4.4 Pad response calculation

Figure 11 shows the position resolution δ utilizing the charge sharing between neighbouring pads as a function of the pad size. Here we use an intrinsic pad response of σ_0 = 5 mm. A two-dimensional Gaussian distribution with width σ_0 was assumed to integrate the induced charge over each pad. Then the center of gravity was computed. The position resolution is defined as the standard deviation of the calculated differences between the original position and the reconstructed centroid.

In addition, noise was introduced on each pad. Here we assume a random noise signal of a certain percentage value of the average pulse height on a pad for a true hit. This percentage value was varied from 0 - 2 % and to illustrate the noise contribution we show its isolated effect on the resolution in Figure 11 as well (dashed lines). We find that a 1 % noise to signal ratio contributes a constant 2 % of the pad size to the resolution in agreement with what has been measured by other experiments. From the input capacitance at the preamplifier, the preamplifier white noise (combined about 1000 electrons) and the typical signal size driven by the dynamic range of the preamplifier (we choose amplification of a factor 1000 of the primary ionization), we find that 1 % is a realistic value for our case. For the calculations we assume the resolution of an 8-bit ADC.

The finite electron statistics is taken into account by superimposing exponential pulse-height distributions of individual electrons. Figure 11 shows the difference in the resolution for 100 and 400 primary electrons for equal contributions from noise (1 %) and from size of the charge cloud on the wire (3 mm).

The position resolution at the pads is computed as a function of the number of electrons n_e and as a function of the size of the electron cloud at the wire σ for a constant noise contribution, a constant pad response σ_0, and pads of 1 cm. The results are shown as points on the left hand side of Figure 12. We find empirically that the resolution can be parameterized by a function $\delta(\sigma, n_e) = 200 + F(\sigma)\exp(-n_e/230)$ with $F(\sigma) = 56.9\sigma + 33.3\sigma^2$ (δ in μm, σ in mm). The right hand side of Figure 12 shows $F(\sigma)$.

In order to calculate the momentum resolution we use this parameterization of the position resolution and add to it the contribution from the non-zero Lorentz angle (stemming from the longitudinal component of the magnetic field as mentioned above).

4.5 Evaluation of momentum resolution

As a first step towards a full tracking simulation the deflection of particles is calculated for two schematic cases of the magnetic field. In case (i) an averaged magnetic field extends over the whole TPC volume and in case (ii) the field is localized to produce a kick in ϕ at the center of the TPC. In both cases the field strengths are chosen for tracks of a given momentum such that the integral deflection in ϕ corresponds to the one for the real magnetic field (at $\theta = 15$ deg. for a 1 GeV/c particle 76 mrad). Note that the effect of the longitudinal field component on the position resolution is taken fully into account. We only approximate how the deflection in ϕ is distributed in z-direction. Reality lies between the two schematic cases (i) and (ii). To reconstruct the momentum from the 14 position measurements a circular trajectory was fitted for case (i) and two straight lines were fitted for case (ii). The difference between the two methods in terms of the resulting momentum resolution is at the 10 % level. The results shown here are for case (i) (averaged magnetic field of 0.17 T).

The original calculated trajectory is circular with a radius of curvature given by the momentum. Space points are generated at 14 positions equally distributed over the 1.5 m length in z of the TPC. These points are smeared according to the multiple scattering inside the gas volume. A 4 cm pad length in z-direction and the track curvature in ϕ at a given z give an original width (σ_α) to the electron cloud (see Figure 3). With this original width of the ionization trail and the transverse diffusion σ_t given in the previous section, the width σ of the electron cloud at the read-out chamber is calculated. For a given cloud width at the read-out chamber and a given number of primary electrons, determined by the gas mixture, the position resolution δ is calculated using the parameterized function shown in the previous section. The additional contribution to the position resolution which comes from the finite time slices of the flash-ADC, the drift velocity, and the Lorentz angle has also been prepared in form of a map and is added in quadrature to the position resolution δ. The 14 position measurements are smeared according to this position resolution. Next, a circular trajectory is fitted to the 14 smeared points to reconstruct the momentum. The standard deviation of the distribution of differences between the original momentum and the reconstructed momentum is defined as the momentum resolution δp.

Figure 13 shows the relative momentum resolution as a function of the momentum for different mixtures of Ne/CO_2, He/CO_2 and $Ar/He/CO_2$. All these mixtures yield a similar momentum resolution at the average momentum of electrons within the CERES acceptance (about 2.5 GeV/c). The values range from 1.5 - 1.8 % and are consistent with the required mass resolution (see CERN/SPSLC 96-35/P280 Add.1).

4.6 Dielectron mass resolution and effect of bremsstrahlung

The effect of material on the momentum resolution of hadrons is mainly due to multiple scattering and has been discussed in detail previously. Electrons undergo multiple scattering as well as energy loss by bremsstrahlung. In this section we discuss the importance of this radiation tail due to the material before the TPC (principally the Si drift detectors, and the two Rich mirrors) on the achievable mass resolution. Calculations were performed using the GEANT framework with materials as in the present CERES/NA45 setup. The mass resolution calculation, in addition to incorporating the bremsstrahlung tails, used the optimized TPC parameters such that a 1% mass resolution is obtained near the mass of the ω meson in the absence of bremsstrahlung. In Figure 14 we show the results for various conditions. All calculations in this figure were performed for the hadronic cocktail as expected and measured for p+Be collisions and with a p_t cut of 50 MeV/c.

Figure 14(a) shows the mass resolution expected neglecting any bremsstrahlung contribution. Figure 14(c) displays the mass resolution one would obtain, were the TPC built behind the presently existing CERES apparatus. The effect of the bremsstrahlung is most clearly visible if one focusses on the components of the spectrum due to the ω and ϕ. For both of these narrow resonances a clear bremsstrahlung tail is visible towards low masses. The full width at half maximum of the resonances is little affected, but in the 700 - 750 MeV mass range, the tail of the ω is difficult to separate from the ρ and the continuum. At 1/10 of the maximum the ω and ϕ widths are increased by about 60 % through the bremsstrahlung tail. On the other hand, the effect on the ρ and and the continuum is essentially negligible. The main contribution to this bremsstrahlung tail is due to the about 4% of a radiation length of the mirror of RICH2, as can be seen by inspecting Figure 14(b) where calculations were performed under the exclusion of the RICH2 mirror. Under those circumstances, the radiation tail only becomes visible at the 1% level of the narrow resonances.

The importance of the bremsstrahlung tail for the physics program with the upgraded CERES detector depends on the precise goals. Inspection of Figure 14(c) (the TPC behind the presently existing CERES apparatus) shows clearly that the two narrow resonances ω and ϕ can still be well separated from the continuum, albeit at a loss in peak efficiency of about 30% . Of course, the scenario underlying Figure 14 is that expected for p+Be collisions, *i.e.* none of the effects such as pion annihilation or vector meson mass shifts are incorporated into this figure. To show what one might expect in a particular model for Pb+Au collisions, we show, in Figures 15 and 16, the results of a calculation of Cassing and coworkers. The calculations were performed including pion annihilation and without (Fig. 15) and with (Fig. 16) shifted vector meson masses. Without mass shifts the pion annihilation significantly decreases the peak/continuum ratio for the ω meson. On the other hand, including the mass shifts changes the ρ region dramatically, but (surprisingly) has very little effect on the ω peak itself (the ω lifetime is 24 fm/c, so part of it should decay inside of the fireball). The pion annihilation continuum is shifted towards lower masses, leading to an actual increase in the peak/continuum ratio for the ω. For both scenarios the ϕ (with a lifetime of about 44 fm/c and with a wave function consisting mostly of strange quarks) is little affected. It should be pointed out that this is just one of the existing theoretical scenarios, and that other scenarios (such as K. Haglin's collisional broadening scenario) might lead to different effects for the ω and ϕ. It is clear, however, that the presence of the ω and ϕ should be measureable for all reasonable scenarios with the resolution depicted in Figure 14(c), *i.e.* with the TPC built behind the presently available RICH2. We also note that the bremsstrahlung tail can be calculated with high precision and unfolded from the measurements.

Summarizing this line of arguments the planned TPC upgrade coupled with the existing CERES apparatus will allow to measure the vector meson resonances ω and ϕ in addition to providing a precision measurement of the dielectron continuum.

On the other hand, the bremsstrahlung tail could be nearly completely removed by replacing the RICH2 mirror in the present CERES setup with a mirror of similar thickness as the present RICH1 mirror. This is demonstrated in Figure 14(d) where the thick RICH2 mirror has been replaced by a 1 % radiation length mirror, keeping all other material unchanged. With this resolution one could not only measure the yield of the vector mesons ω and ϕ, but also search for small changes in their line shape, resulting from possible mass changes. In addition, we would like to point out that in the absence of precise theoretical predictions for the shape of the dielectron spectrum it is prudent to try to build the upgrade with the best possible mass resolution achievable. For this reason we are presently also investigating the possibility to replace the mirror of RICH2. A suitable candidate for such a mirror would be one built from a carbon fiber laminate substrate, coated with Al + MgF_2. Mirrors of this type and of the appropriate thickness (1% of a radiation length) have been looked at in the course of the preparation of the HADES experiment at GSI (J. Friese, private communication). Following this experience it seems feasible to build a mirror of the required size and thickness within a time scale of about one year and within a budget of less than DM 300,000. The CERES collaboration plans to pursue this possibility. However, we wish to reiterate that the major physics goals for the proposed upgrade can be realized with the apparatus as is presently proposed, *i.e.* with a radial TPC behind the *existing* CERES detector.

4.7 Tracking

Presently, in CERES electrons are tracked in CERES/NA45 using the two-dimensional position measurement in the two Si-driftchambers and the angle measured in RICH1, the angle in RICH2 (after the ϕ kick in the magnetic field), and the two-dimensional position measurement in a pad chamber at the downsteam end of the spectrometer. The entrance to the TPC will be at the location of the pad chamber. To demonstrate the density of hits at the entrance of the TPC, we show in Figure 17 the distribution of hits in the padchamber from a typical central Pb + Pb collision. In this event we find 280 clusters. This multiplicity is well in line with the distributions presented by NA49 at Quarkmatter '96 taking into account in addition conversions and results for shower leakage from the radiator vessels and coils (using GEANT). These two sources increase the total number of hits in the padchamber by 20 % as compared to the multiplicity of primary charged particles entering the acceptance. This sets the stage for judging the occupancy in the TPC. It should also be noted that the hit density is quite uniform over the acceptance in polar angle of $\theta = 8 - 14.5$ deg., corresponding to pseudorapidities of η = 2.06 - 2.66, i.e. just backwards of midrapidity (y=2.90).

The momentum of charged particles will be measured in the TPC, while the present CERES spectrometer (without the padchamber) will give the vertex position, emission angle, and, for electrons, double particle identification (in both RICH counters) and a first momentum measurement. To illustrate that the connection between the present CERES spectrometer and the TPC will not be a problem, we show in Figure 18 the pointing capability of the present spectrometer. In the top of the figure is shown the distance between a hit projected from the upstream tracking and the actual position of the closest hit. The pointing resolution in x and y is given by a standard deviation of 0.7 pad units or 5.3 mm. To put this number into perspective we also show, in the bottom of Figure 18, the distribution of distances from a hit to the next neighboring hit. With a standard deviation of 3.6 cm in x and y it reflects the relatively low hit density. Searching, as done presently, an area of $\pm 1.5\sigma$ in x and y for the matching hit, the probability for an accidental match is just below 5 %.

The occupancy in the TPC is low. For every slice in z the number of readout cells is 10,000 divided by 14 (slices in z) times 256 (time bins), i.e. 183,000. For 280 charged particles entering the TPC, 280 times 3 (pads) times 3 (time bins) = 2520 cells or 1.4 % will be occupied. There will of course be hits not associated with actual tracks. The present experience of NA49 shows about twice as many hits as can be matched with actual tracks. If we assume the same scenario this still leaves us with an occupancy below 3 %. This corresponds to the occupancy in the most dilute regions in the NA49 TPC's at the largest angles, while there the occupancy at small angles reaches values of 20-30 %. Taking as example the equivalent numbers for the NA49 VTX2 TPC's, 197,000 readout cells in a z slice are occupied by 700 (charged tracks) times 2.5 (pads) times 7 (timebins) times 2 (additional hits) leading to an average occupancy of a cell of 12 %. NA49 can successfully track in this environment and this makes it plausible that in our TPC finding the hits matching to a track will not be difficult.

The magnetic field, although rather nonuniform, will be known (measured) and we do not see where this poses a major difficulty for the tracking.

In terms of general tracking strategy we see two possibilities. Our main goal is to track electrons. For these, the TPC provides a second, improved measurement. It would be natural to start with the predictor from the upstream spectrometer. In that case, only a small fraction (typically 5 %) all track candidates in the TPC will have to be processed. The efficiency will be limited by the requirement to have two times two clean ring signals in the RICH counters and a pointing accuracy as indicated above. The additional CPU time per event would be small compared to the present time of about 5s (since most of this time is spent to find the vertex from the ca. 250 hits in each Silicon driftchamber. The other possibility is to start from the TPC and point into RICH2 for electron candidates. In that context the developments of NA49 using templates on two-dimensional information is interesting for us. For our application one can think of slices of constant polar angle θ to apply the template to, since the deflection is mostly in azimuth ϕ. The templates would only serve to find the hits that belong to a given track, the momentum is calculated precisely in three dimensions (as in NA49). We have not evaluated the implication in terms of CPU time. Independent of the tracking strategy we will only further analyze events with at least two stiff electron candidates which reduces the data sample to 1/5 of the events or less.

4.8 Gas system

The total volume of the TPC which extends upstream and downstream approximately 4 cm beyond the field cage is about 7 m^3. While the gas will be recycled about 10 % of new gas will be added each day. This means that for a running period of 42 days and a set-up time of similar length for purging and calibration of the detector a total of about 70 m^3 of gas will be needed. The gas volume will be exchanged once per day. Hence, the flow rate will be moderate at around 5 l/min. Our requirements for the gas system will be similar to that of NA49: a recirculating system with continuous removal of oxygen and water to 1-2 ppm levels, moderate flow rate, a well defined mixture of noble gas and quench gas (in our case CO_2). We have been in contact with Mr. Bosteels about the gas system and envision that it will be built by him.

4.9 Mechanical design

Detailed mechanical design drawings of the TPC including the read-out chambers, the module holders, the field cage, and various support structures have been produced and handed over to the referee for his reference and information.

5 TPC Front End Electronics

This section contains a summary of the specifications for the front-end electronics for the TPC. The basic design parameters are given in the following table.

gas mixture	90% Ne/ 10% CO_2
drifttime	71 μs
drift velocity (near readout chamber)	4 mm/μs
long. diffusion (σ_l)	0.8 mm to 2 mm
number of readout channels	10000
number of time slices	256
padsize	$4 \cdot 1 \times 1$ cm^2
noise (pad capacitance typ. 30 pF)	< 1000 e$^-$
signal to noise	100:1
dynamic range	250000 e$^-$
resolution	8 bit
readout time	< 500 μs

At the moment we are considering four different options:

(i) A design based on the front electronics developed for the STAR-TPC.

(ii) Development of our own preamplifier/shaper-chip to optimize shaping time and power consumption.

(iii) Modification of the STAR SCA/ADC-chip to reduce settling and reset time.

(iv) Design our own SCA/ADC, eventually with the preamplifier on the same chip.

In the next section we describe the performance of the STAR electronics for our purposes and emphasize the necessary compromises which arise from the different specifications of STAR and CERES. The remaining two sections describe briefly our present thinking about possible own electronics developments.

5.1 LBL Front End Electronics for the STAR TPC

The developments of a readout system for a TPC detector carried out at LBL since many years are finished and successful operation has been proven within the NA49 experiment. The front end modules consist of two full custom ASICs: (i) a 16 channel charge-sensitive preamplifier with tail correction and semigaussian shaping (SAS) and (ii) a 16 by 512 channel switched capacitor array with a Wilkinson type ADC for each channel (SCA/ADC).

The SAS equivalent noise charge is about 900 e^- (rms) at input pad capacitance of 15pF. The overall chip gain is 16mV/fC with a dynamic range of up to 2 volts. This means that the required signal to noise ratio of 100:1 can be reached with a moderate gas gain of 500. The dynamic range required is around 250000 e^- which corresponds to an output signal of 650 mV, again within the STAR SAS-chip specifications. The SAS-chip offers adjustable shaping and tail correction time constants. The maximum adjustable shaping time of th SAS-chip is 150 ns (FWHM). Due to the larger spread in arrival time of the signal (σ 200 - 500 ns) of our setup this gives rise to some input signal loss, which has to be compensated by a higher gas gain. The tail correction can be nicely tuned for our purpose as the necessary time constant is within the bracket of the design values required for STAR. One additional drawback is the large power consumption of 60 mW per channel which is mainly (70%) caused by the output buffer. The chip is fabricated in a 1.2 μm CMOS technology (ORBIT) and we can purchase it in a PLCC package completely tested.

Our main concern is the rate capability of the SCA/ADC-chip. Measurements at LBL, together with experts, revealed that the Wilkinson ADC can be operated at count frequencies up to 190 MHz. Although the clock distribution is very delicate (the duty cycle must be controlled with an 0.5 ns accuracy) a slightly more "moderate" conversion frequency of 150 MHz leads to an average conversion time of 900 ns per channel at 8 bit resolution. The ADC limits the achievable dynamic range to 600 mV. The noise of the SCA/ADC is slightly higher compared for our application as compared to the operating conditions STAR is envisioning.

The main bottleneck, however, is the settling and reset time (1.2 μs + 2.2 μs) of the operational amplifier which buffers the ADC input. To be compatible with the readout time of the other detectors we have to use two SCA/ADC-chips with 128 time samples each. The overall acquisition time is then 71 μs (drift) plus 550 μs (readout). From this it is clear that the readout speed is marginal as compared to our goal. The SCA/ADC-chip also comes in a 84 pin PLCC package and will be delivered fully tested.

The design of the additional electronics and of the front end boards is, although not trivial, achievable for 1998 data taking. The interface to the data acqusition will be based on our own developments for the RICH-detectors and the silicon drift chamber. This concept has proven to work and, as one of the main design goals, is equally well suited for other detectors.

5.2 CERES Preamplifier Development

Recently we have developed a charge sensitive preamplifier with shaper and differential output stage for silicon drift detectors. This design was performed in a modern BiCMOS-technology and is currently being tested at Heidelberg. Although the requirements are different for a TPC, the basic concept is rather similiar. Based on this experience we have already started with the design of a preamplifier which is suited for the higher input capacitance and the longer shaping time. The input stage is comprised of a PMOS input transistor, which has a huge aspect ratio to maintain capacitive matching to the pads, and is followed by a semi-gaussian shaper. The tail correction will be performed in either the classical pole-zero cancelation technique or a filter network similiar to the SAS-design. Our technology (AMS 1.2 μm BiCMOS) offers, in addition to the CMOS-process, bipolar transistors which allows to reduce the power consumption to 10 - 15 mW per channel. The noise will be similiar to the SAS-chip, it could be slightly better because of the lower flicker noise of this technology compared to the ORBIT process. The shaping and tail correction time constants will also be adjustable since the final choice of gas is still open (He-Ar vs. Ne). It is planned that one student and one experienced designer will work continously on this design for the next year.

5.3 Modification of the STAR Switched Capacitor Array and ADC circuit

As mentioned before the buffer of the ADC limits the rate capability of the LBL-design. This finally would hinder us to reach the minimum deadtime of 300 μs, which is given by the RICH-detector readout. At the moment we negotiate with LBL to deliver us the schematics and design files of this chip. This woulds enable us to modify the relevant parts and submit the revised design to industry. In case this is not possible, for whatever reason, we already started to search for available SCA-designs at other research laboratories and universities. A very nice design, which is public domain, has been fabricated at the ASIC-workshop at University of Heidelberg. It was developed for the HERA-B experiment and is, with some modifications, usable for our needs.

6 Schedule

Figures 19 - 22 show our present schedule to complete the construction of the TPC in time for tests with protons in 1998 and participation in the 1998 heavy ion run. We envision the 1998 ion run to be first an engineering and tune-up run, followed by an initial production run. Full production runs of six weeks each should take place in 1999 and 2000, one at low energy and one at full SPS energy.

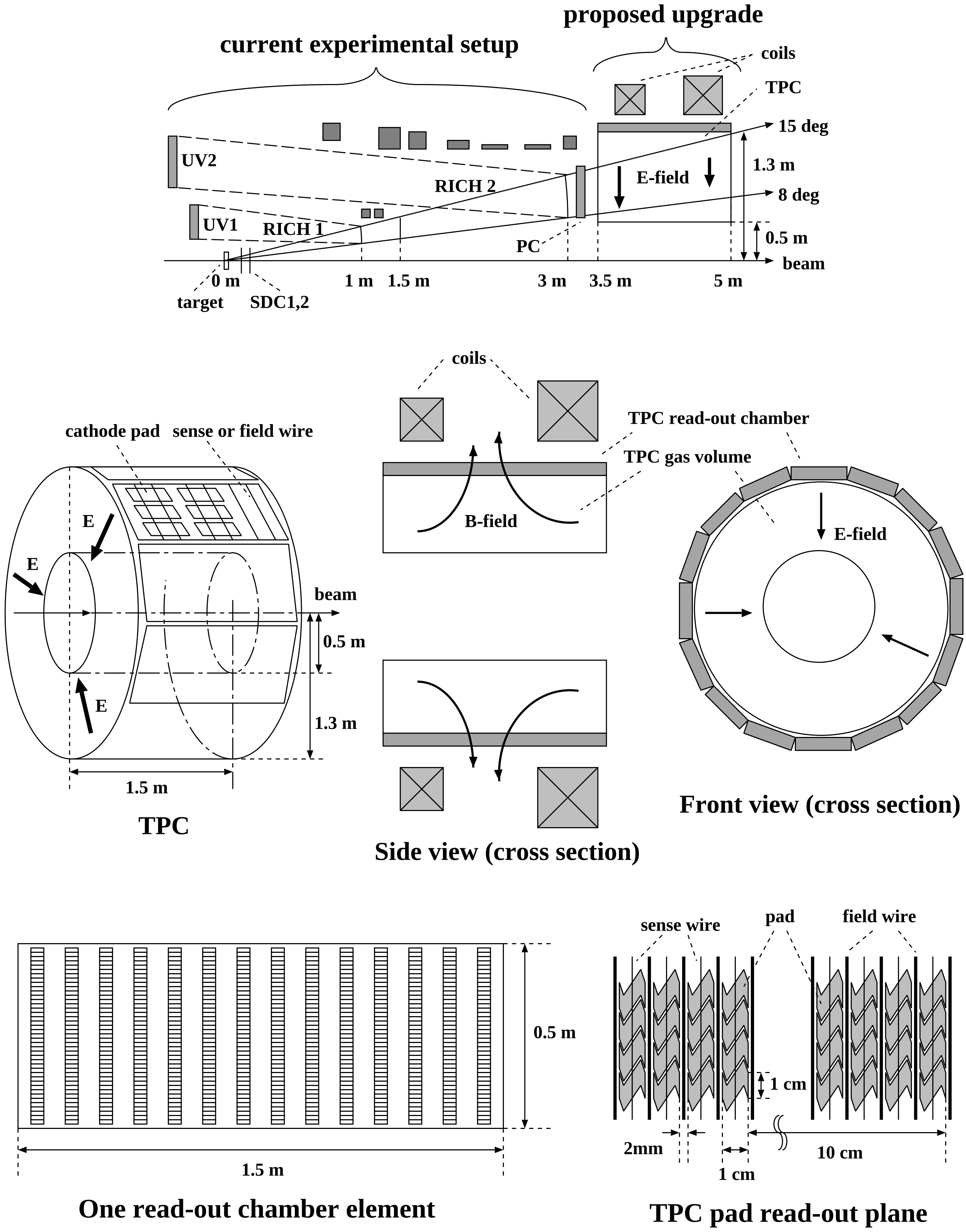

Figure 1: Lay-out of the proposed CERES upgrade

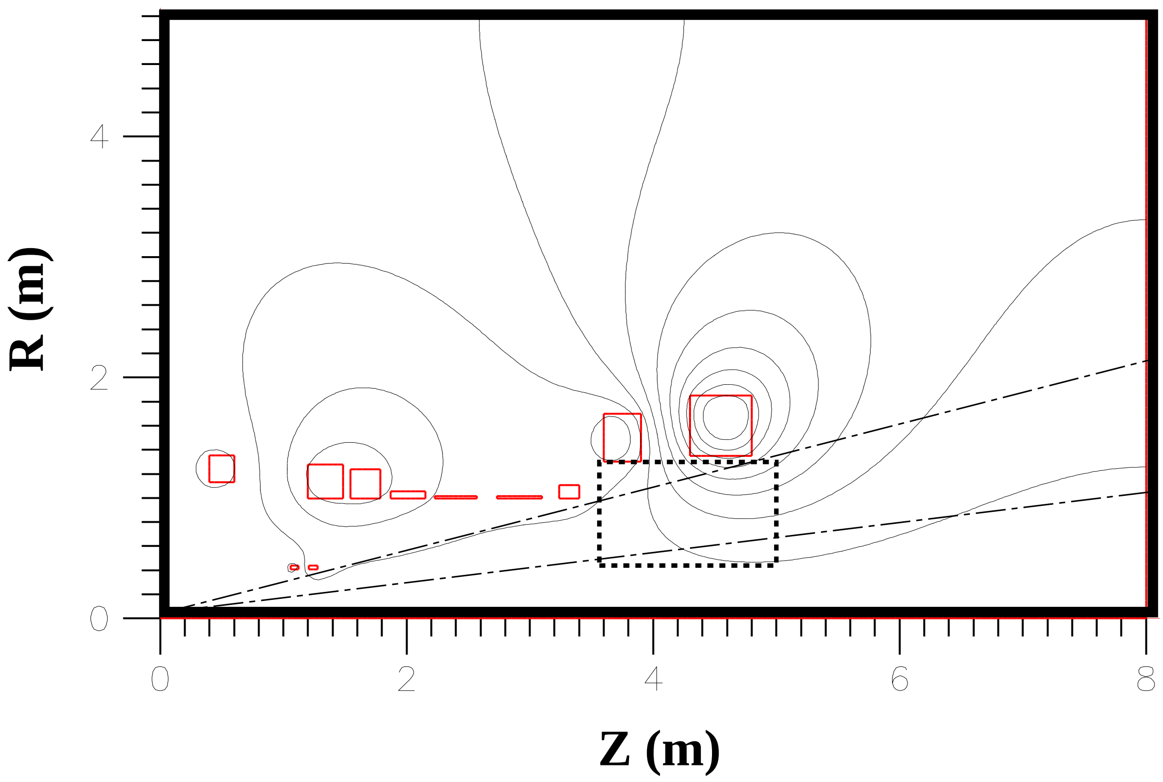

Figure 2: Calculated magnetic field lines for the combination of the existing CERES spectrometer and the additional analyzing coils in the TPC region. The active volume of the TPC is indicated by the dashed rectangle.

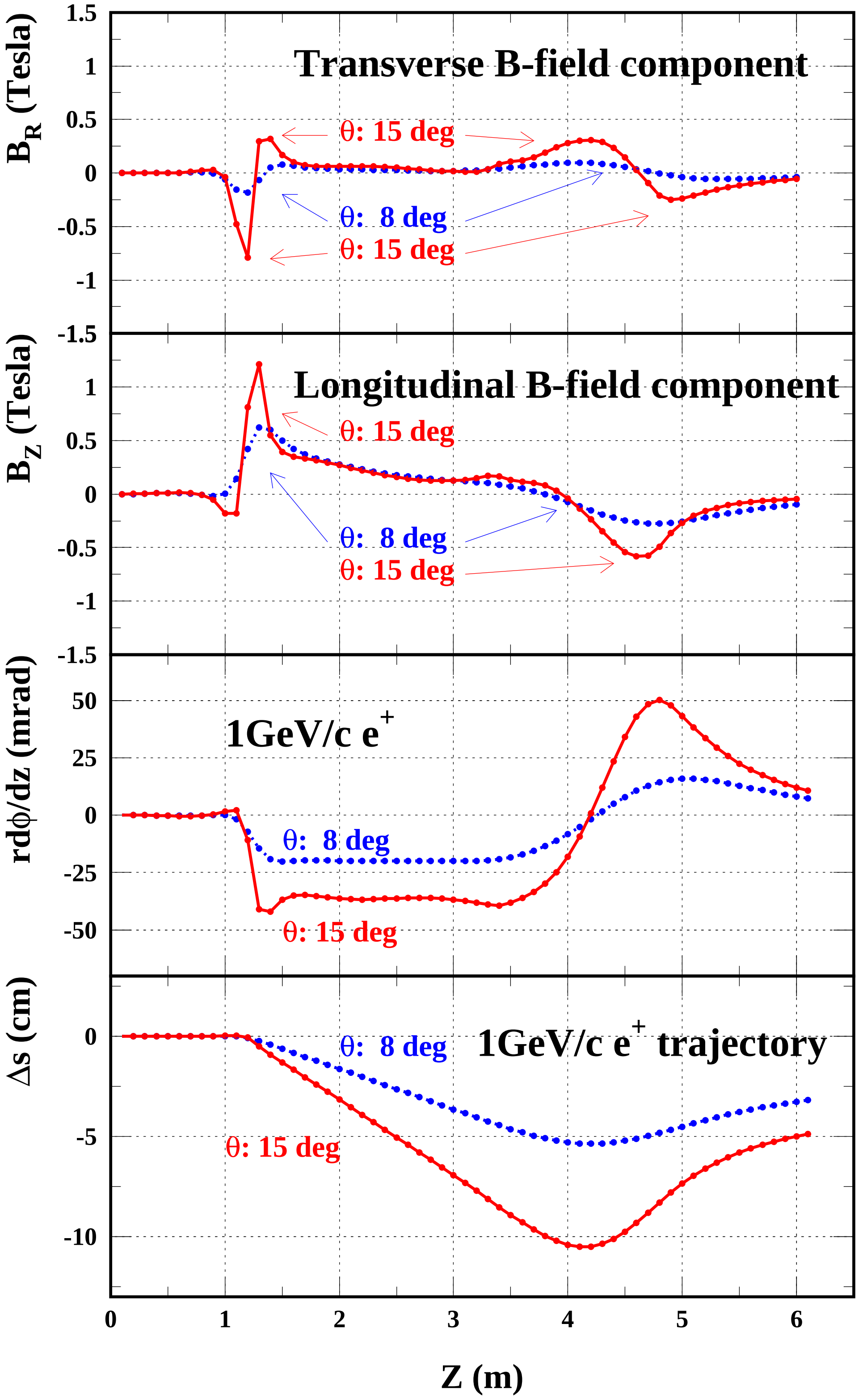

Figure 3: Magnetic field components transverse to and in beam direction (top and next to top) as well as a displacement from an undeflected track on the surface of a cone with angle θ of a 1 GeV/c singly charged particle (bottom). In the next to bottom plot is shown the length of the arc projected into the r-ϕ plane per unit length in z, r$\cdot$dϕ/dz.

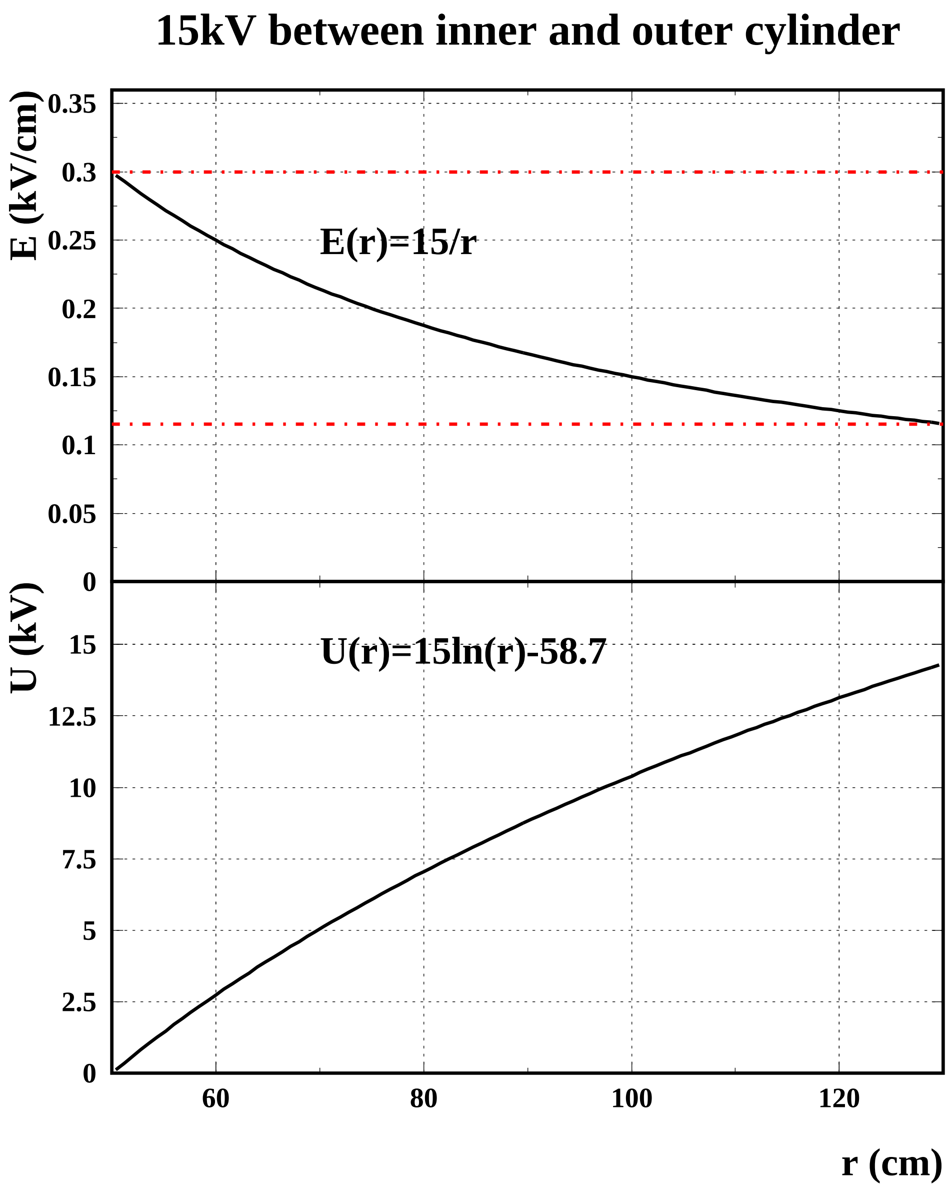

Figure 4: Electric field and potential in the TPC as a function of radius r.

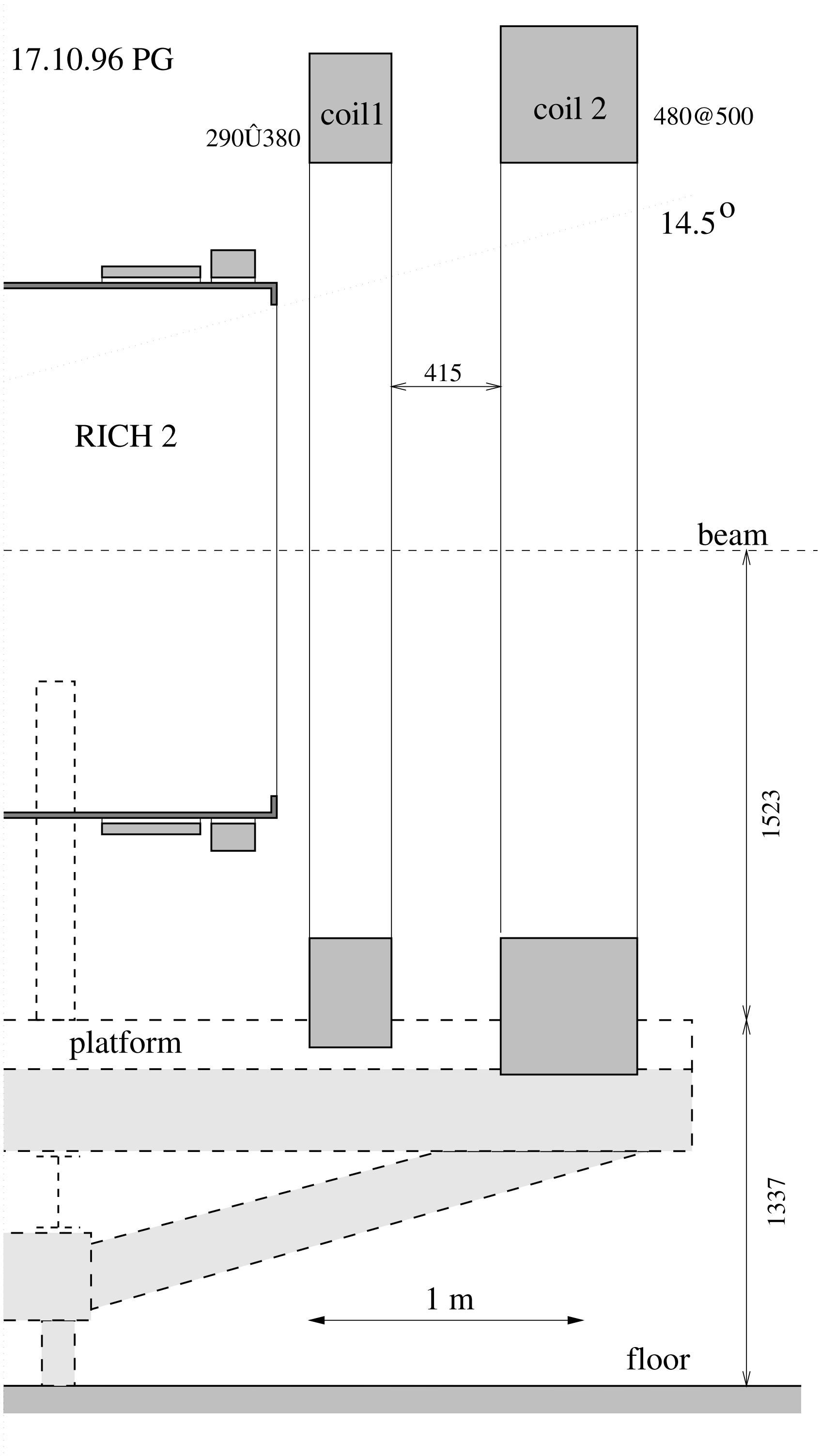

Figure 5: Side view of RICH2 and TPC magnet

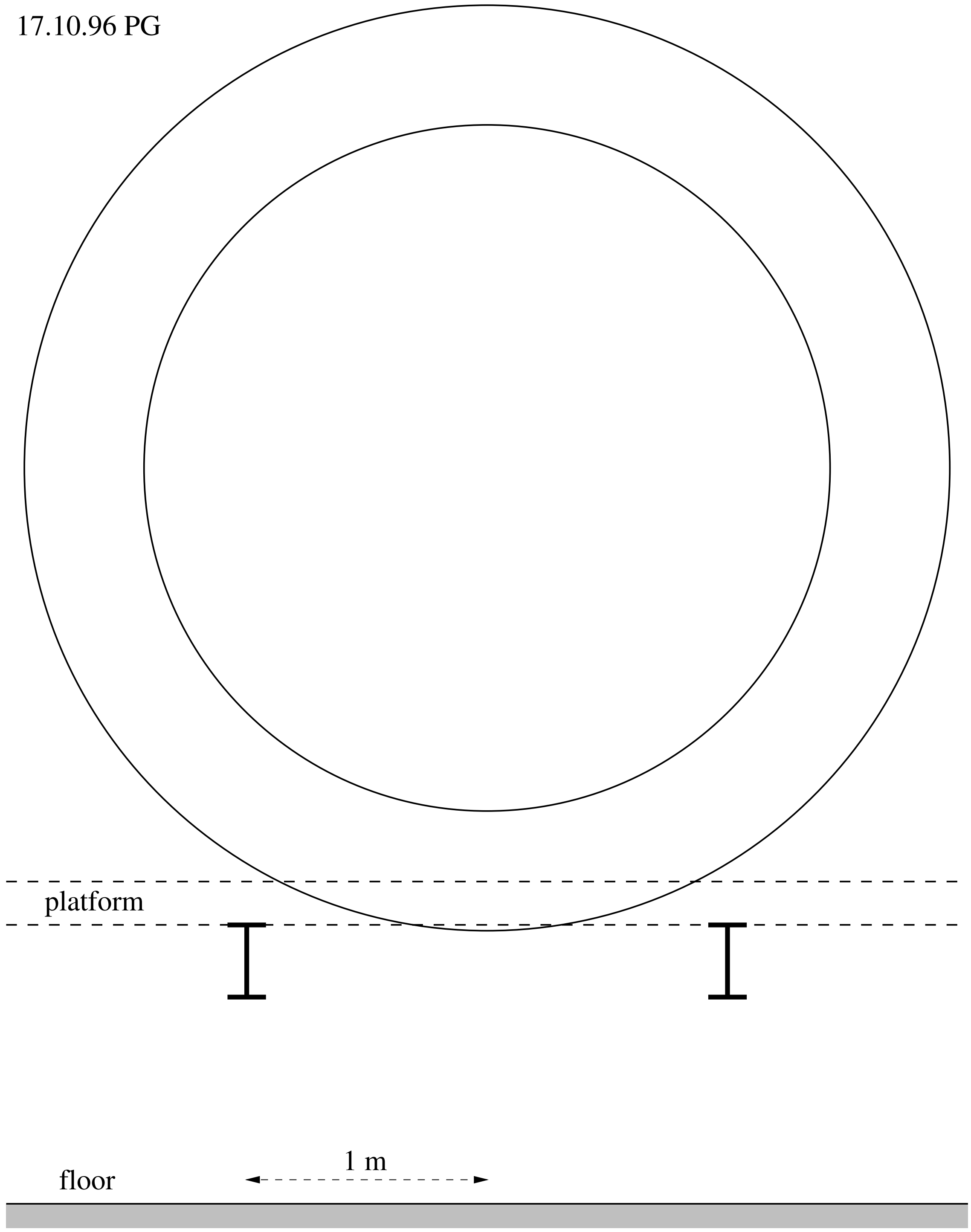

Figure 6: View against beam, showing the location of the support beams of the platform with respect to the TPC magnet coils

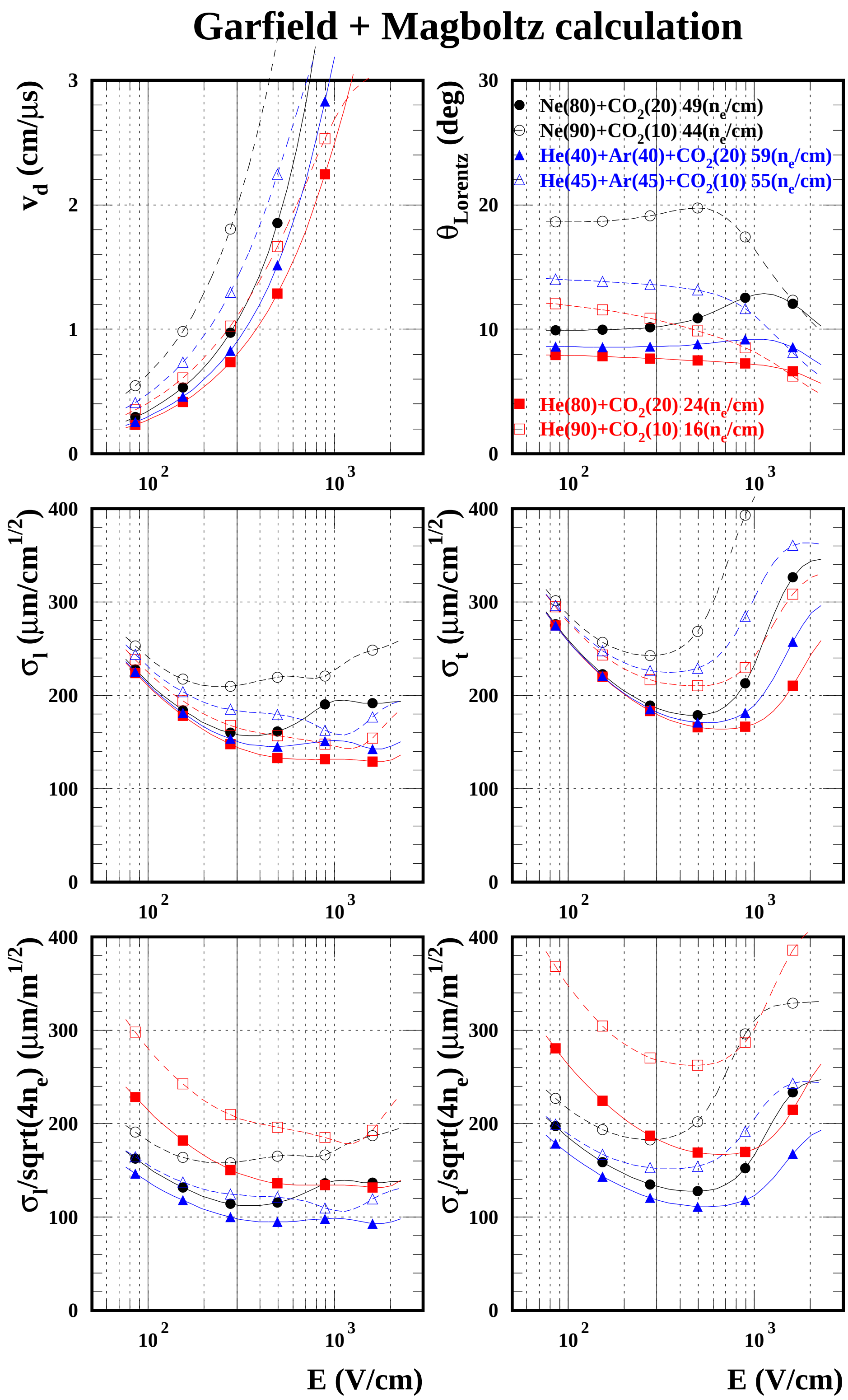

Figure 7: Drift velocity (top left), Lorentz angle (top right), longitudinal and transverse diffusion constants (middle) and longitudinal and transverse diffusion constants normalized to the square root of the number of charge carriers (bottom) for different mixtures of noble gas and CO_2.

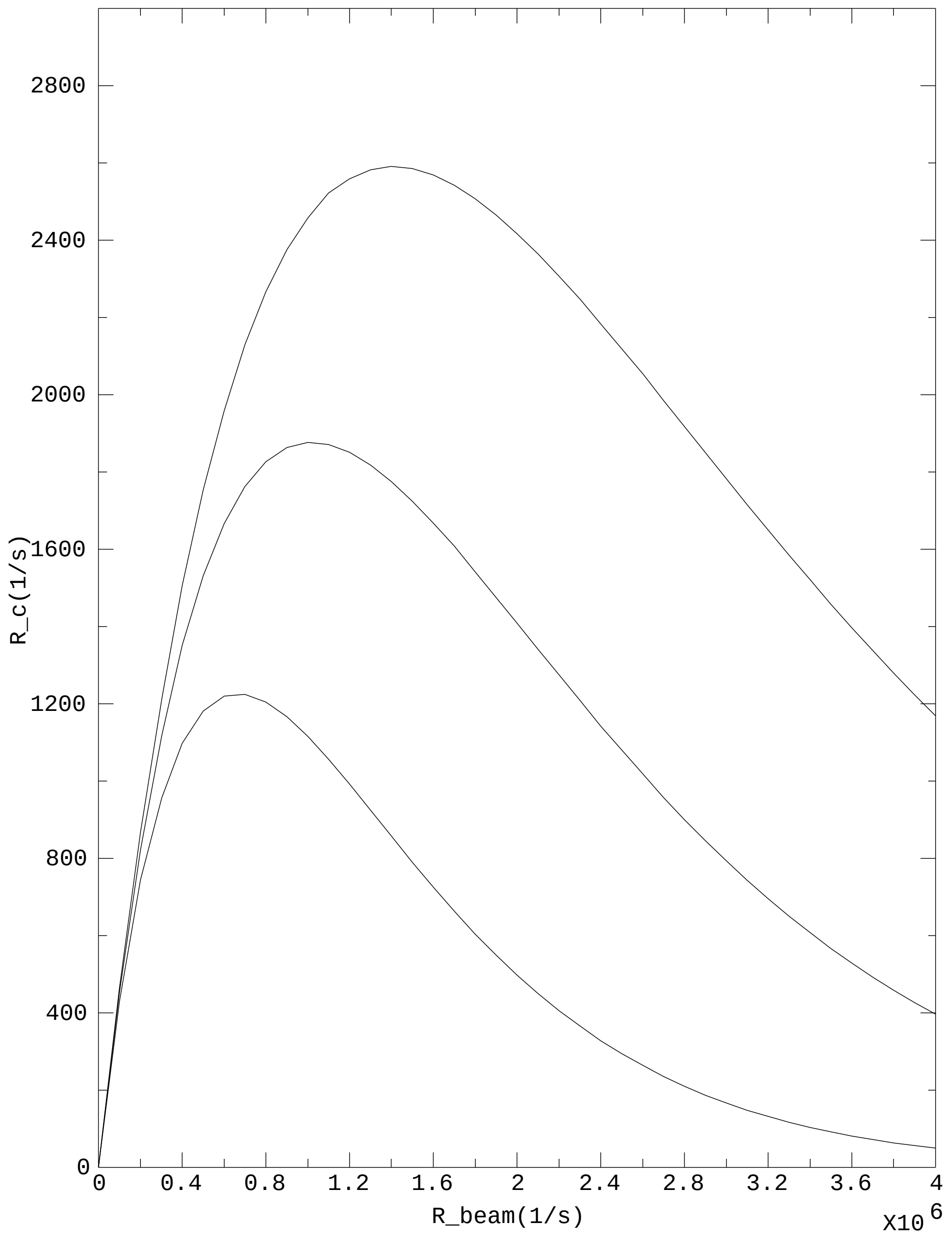

Figure 8: Rate of clean interactions (for definition see text) as a function of the beam intensity. The three curves are for drifttimes of 71 μs (top), 98 μs (middle), and 150 μs (bottom).

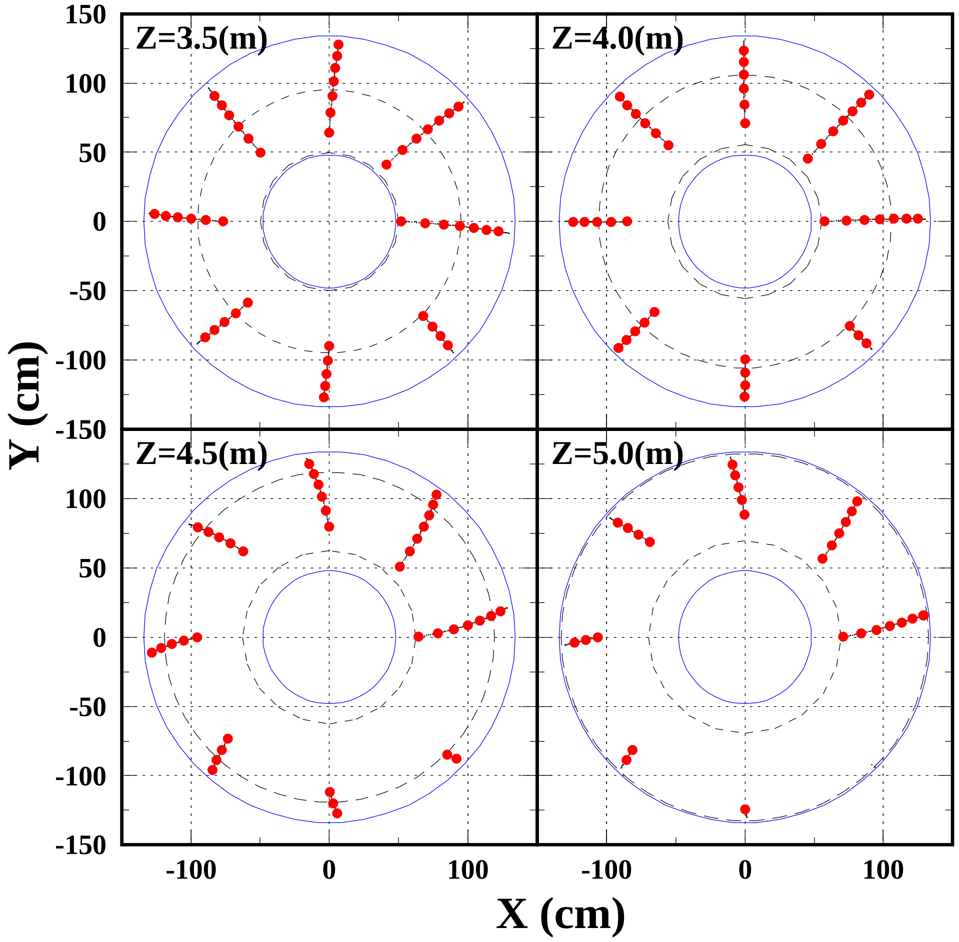

Figure 9: Trajectories of electrons drifting in the electric and magnetic fields in the TPC at four different locations in z.

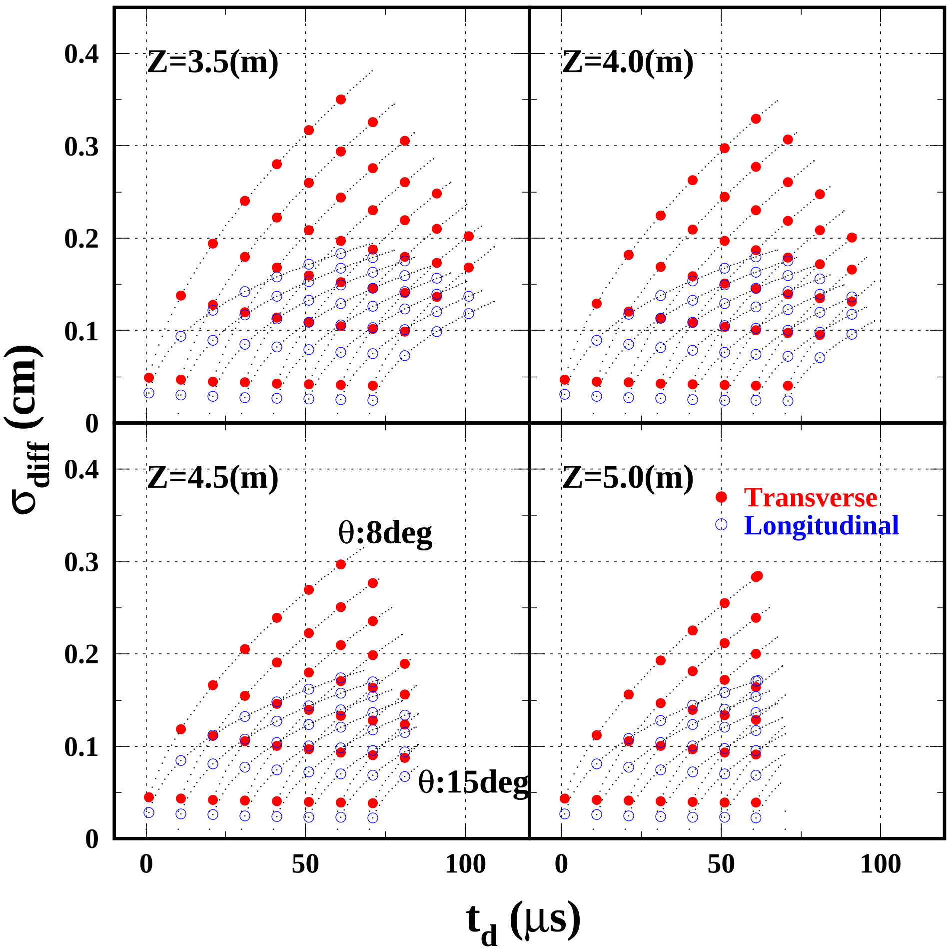

Figure 10: Diffusion of the electron cloud transverse to and along the drift direction for primary ionization at polar angles ranging from the minimal to the maximal in 1 degree steps (different calculations displaced horizontally by 10 μs for better visibility).

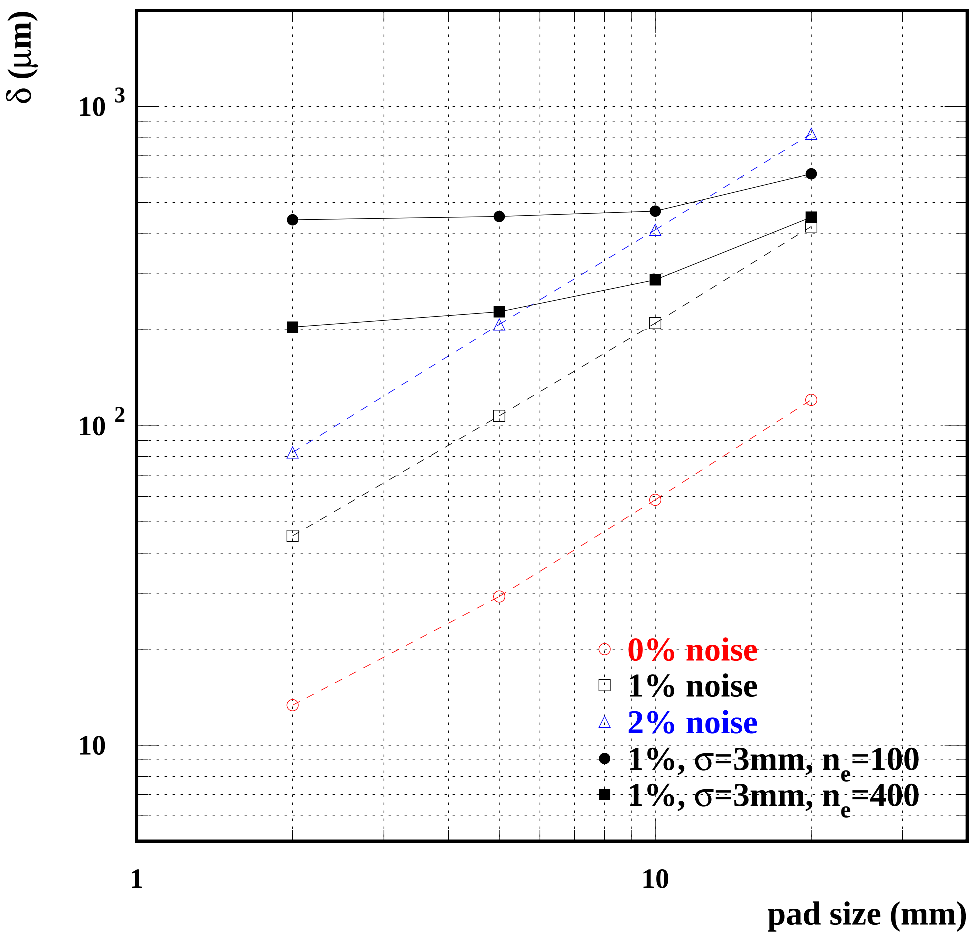

Figure 11: Resolution in ϕ direction from charge division between pads as a function of pad size. Curves are shown for different noise contributions without taking account the spatial extent of the charge cloud (dashed lines) and for 1 % noise and spatial extent of the charge cloud assuming different numbers of primary electrons (solid lines).

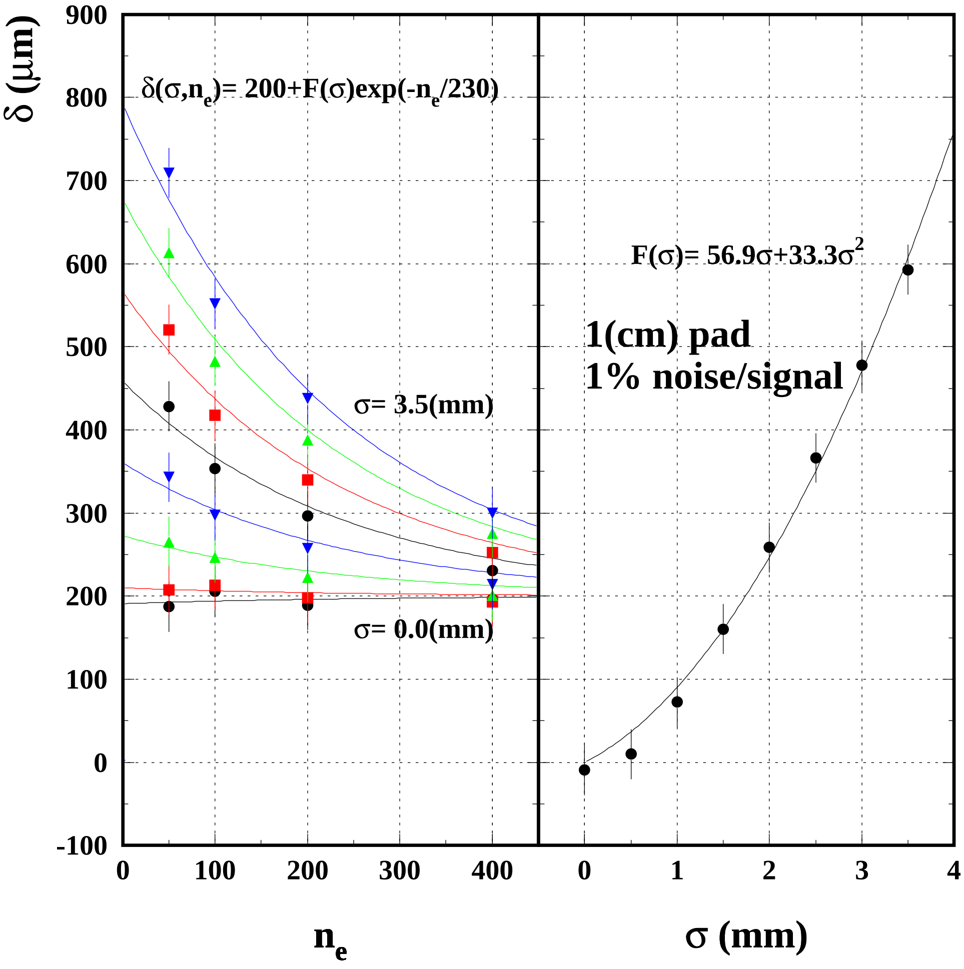

Figure 12: Resolution in ϕ direction from charge division between pads as a function of the number of primary electrons (left) and as a function of the width of the charge cloud at the sense wire (right). The solid lines result from the empirical parameterization discussed in the text.

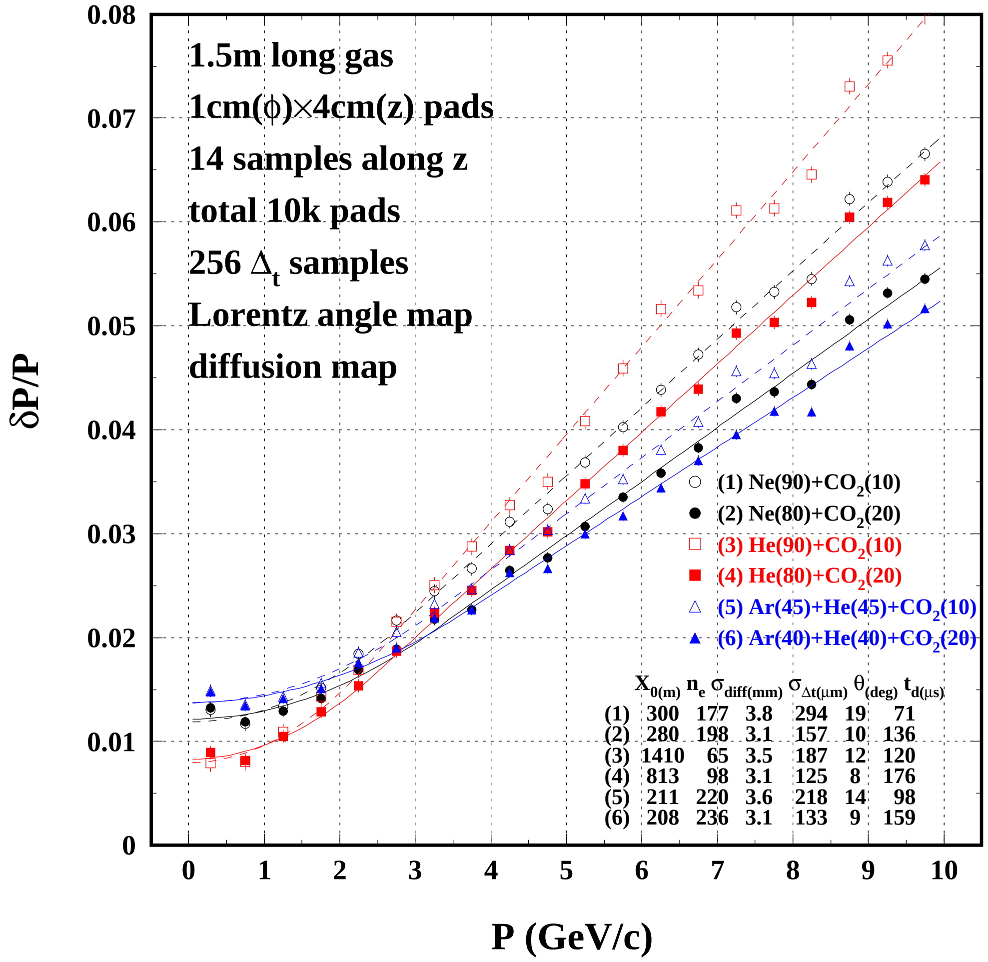

Figure 13: Momentum resolution of the proposed radial TPC.

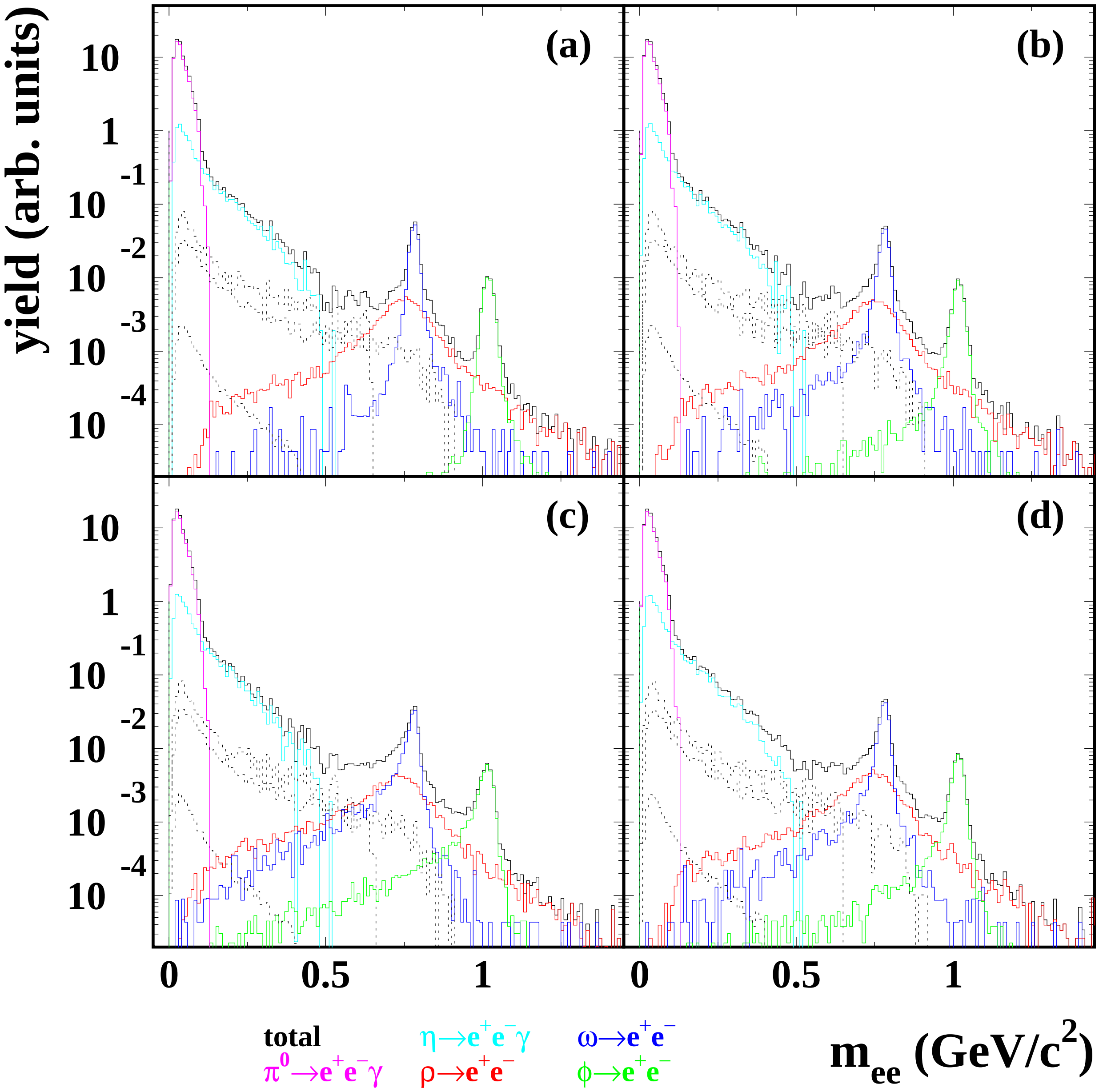

Figure 14: Dielectron mass resolution of the proposed radial TPC. Part (a) shows the spectrum without inclusion of bremsstrahlung. Part (b) includes bremsstrahlung in all CERES/NA45 material except the mirror of RICH2, while in part (c) the mirror of RICH@ is also included. Part (d) is a calculation with a hypothetical 1 % of a radiation length thick RICH2 mirror and all other material unchanged.

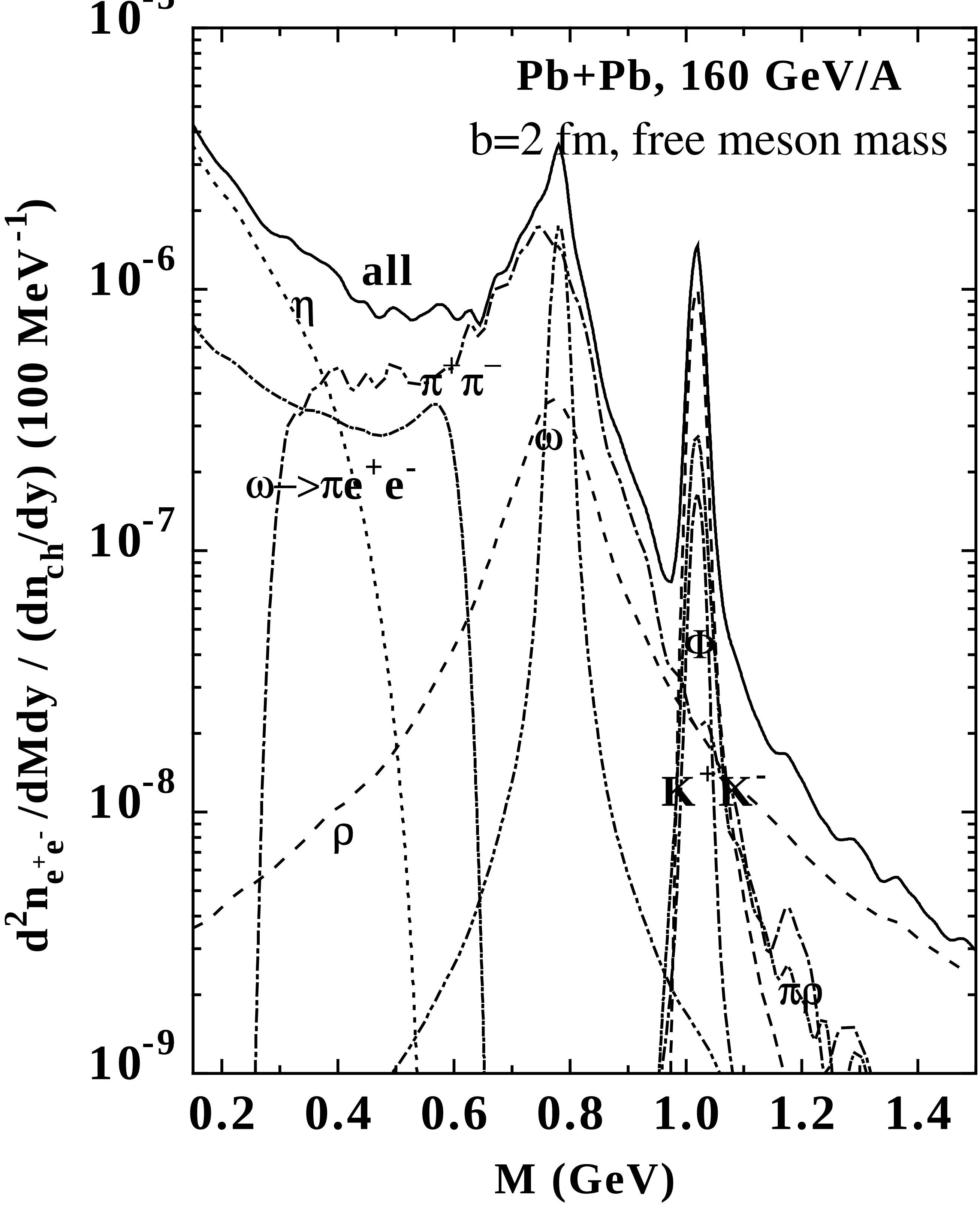

Figure 15: Dielectron mass spectrum of Cassing et al. No mass changes.

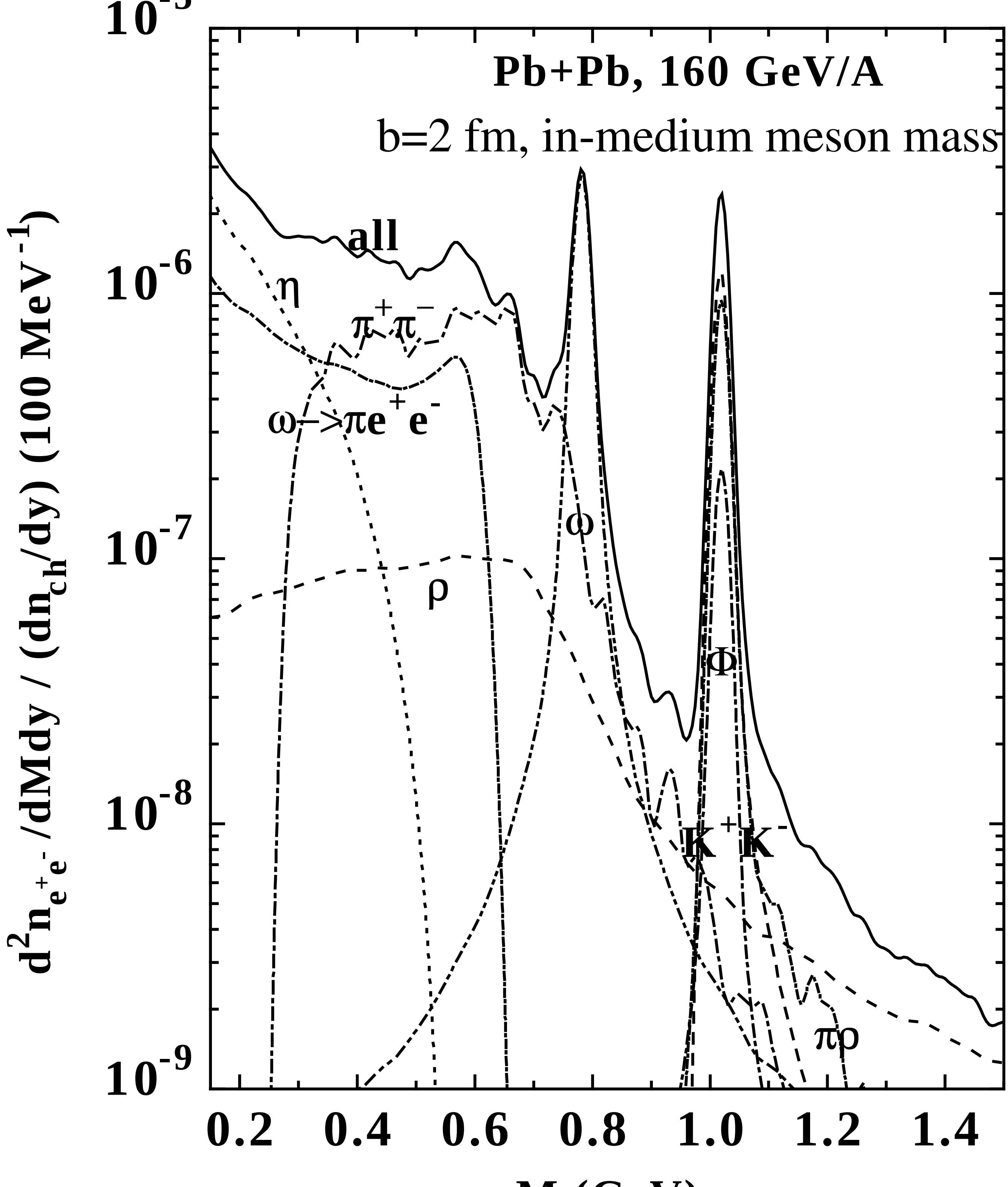

Figure 16: Dielectron mass spectrum Cassing et al. In medium mass changes are included.

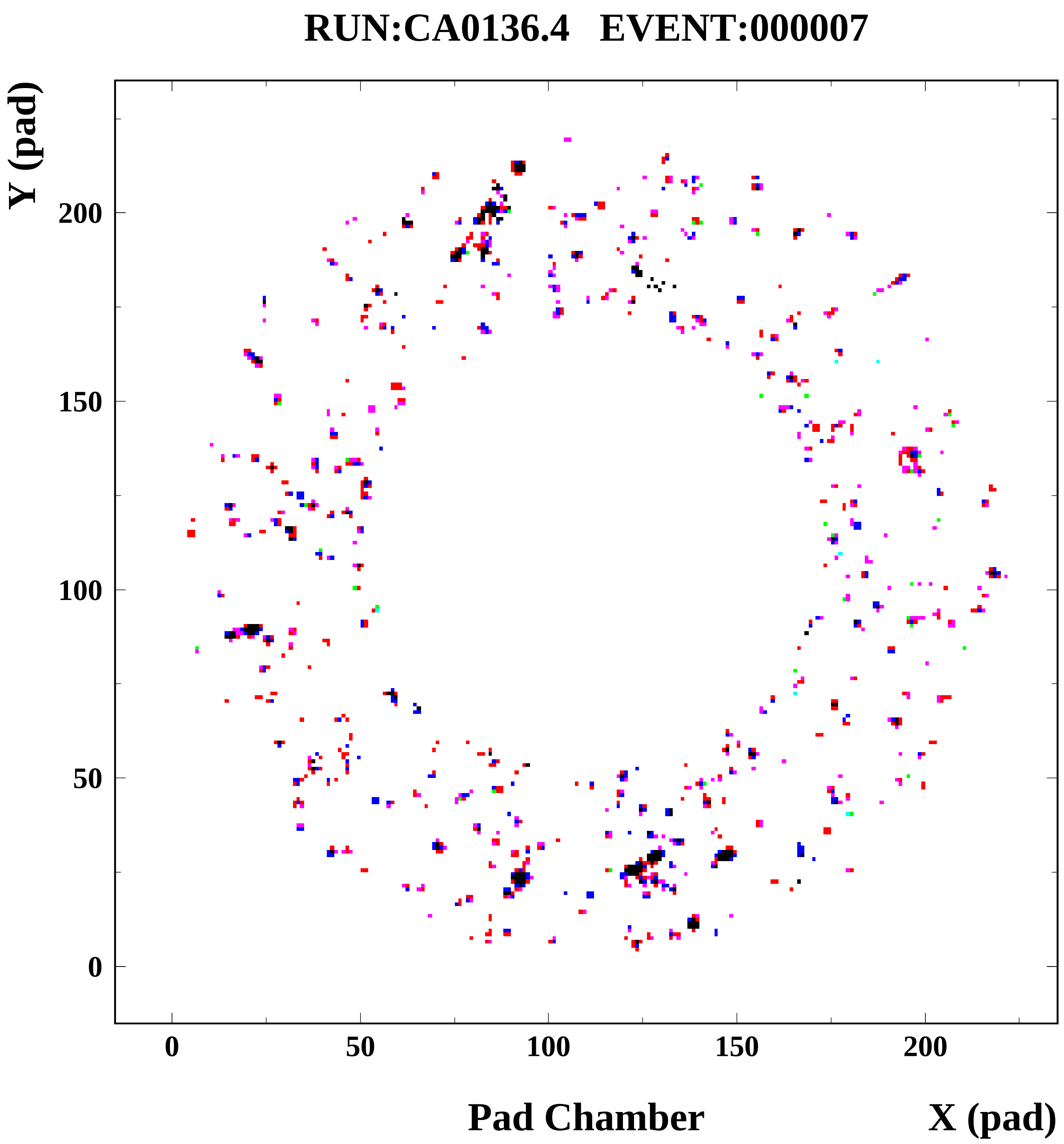

Figure 17: Event display in the padchamber for a central 158 A GeV/c Pb + Pb collision.

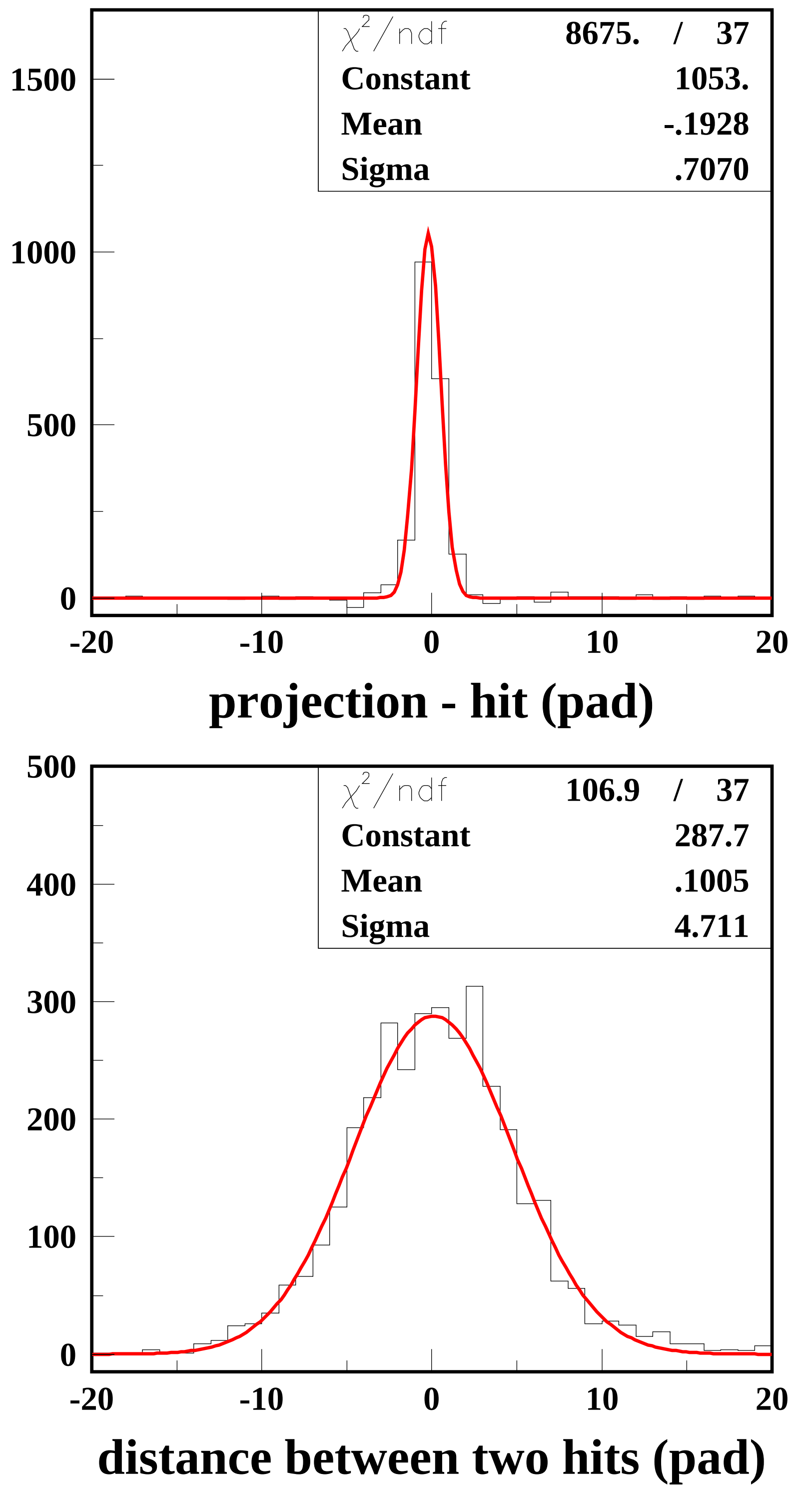

Figure 18: Top: Pointing capability from Si-drift chambers and RICH detectors into padchamber (equivalent to entrance of TPC). One pad unit corresponds to 7.6 mm. Bottom: Average distance of tracks at padchamber (entrance of TPC), again in units of 7.6 mm.

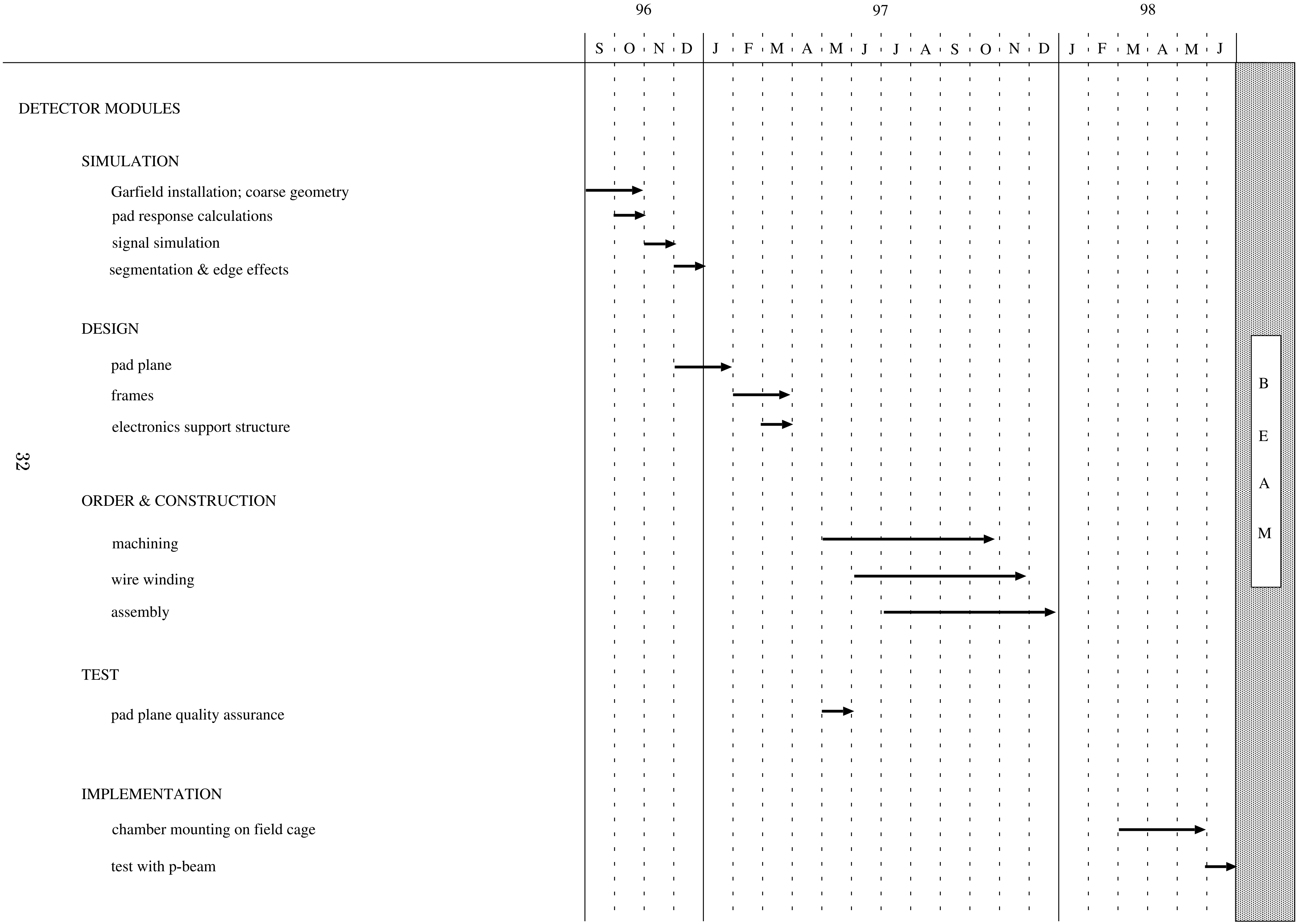

Figure 19: Schedule for read-out chambers

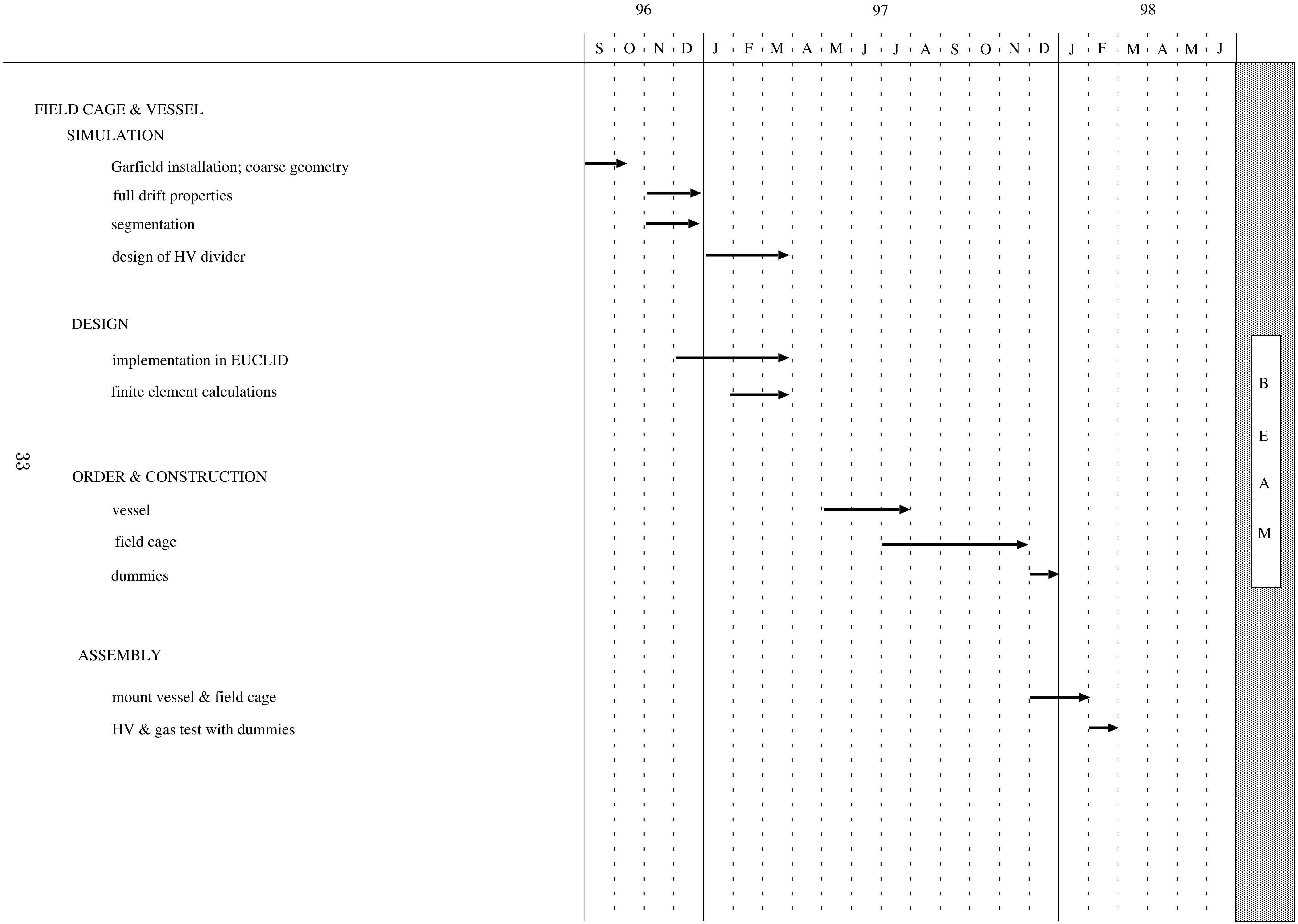

Figure 20: Schedule for main vessel and fieldcage

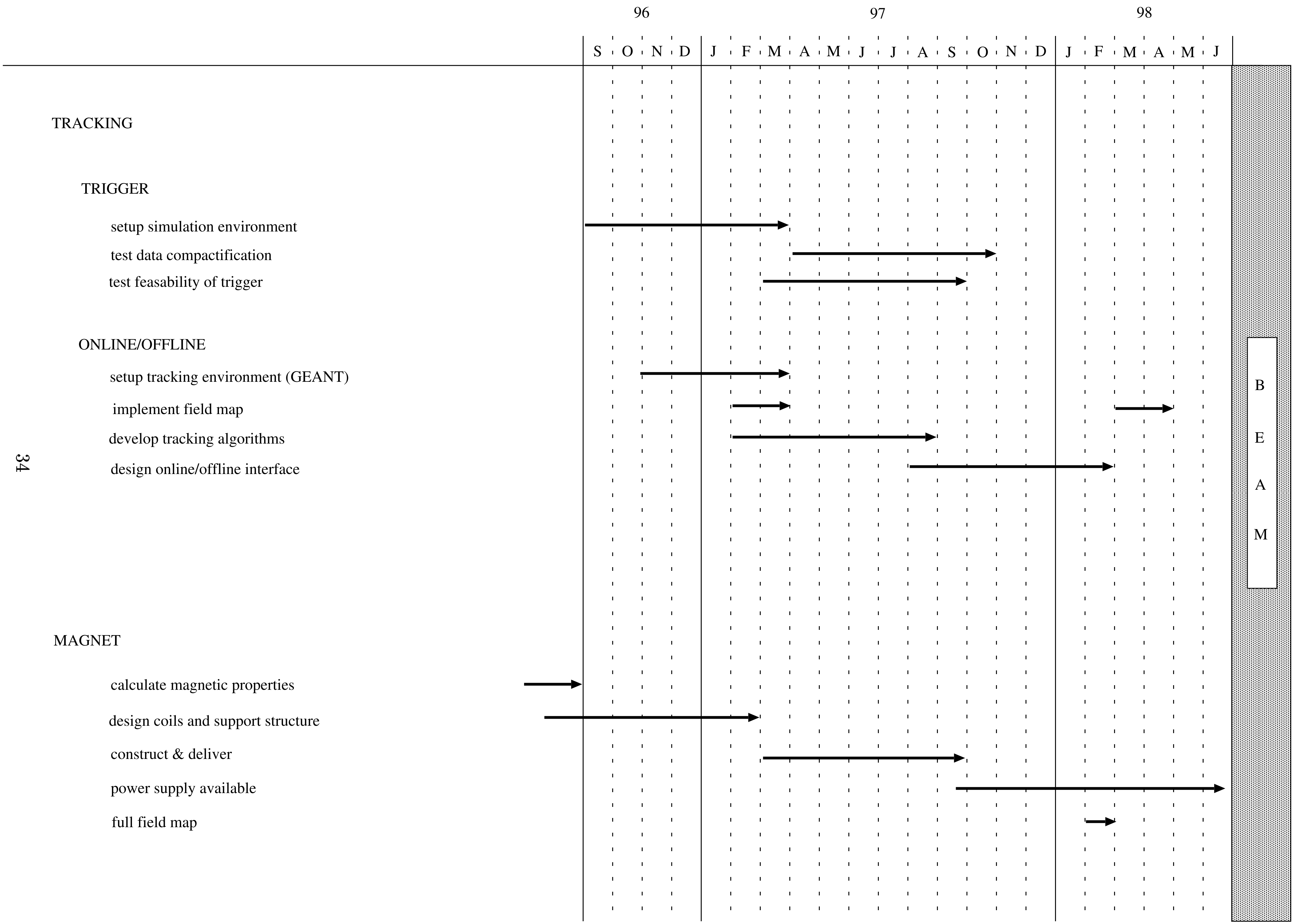

Figure 21: Schedule for tracking simulation, software development and magnet